

Galactic Archaeology with RAVE: Clues to the Formation of the Thick Disk

Indranil Banik, Georges Kordopatis, Gerry Gilmore

December 3, 2024

Contents

1	Introduction	3
1.1	Constraining Stellar Ages From Distant Observations	4
1.2	Disk Heating & Radial Migration	4
2	Methods	5
2.1	Datasets & Selection Criteria	5
2.2	The Co-Ordinate System	9
2.3	Monte-Carlo Procedure & Binning The Data	10
2.4	Parameter Extraction & Error Budgets	11
2.4.1	Dangers Of Small Sample Sizes	11
3	Results	13
4	Toy Model	22
5	Discussion	25
6	A Natural Scenario for the Formation of the Thick Disk	26
6.1	Dynamics of the Milky Way and Andromeda galaxies	26
6.1.1	Dynamics in an Expanding Universe	30
6.2	The Geometry of a Flyby of Andromeda	31
6.2.1	The Impulse Approximation in the Deep-MOND Limit	36
7	Conclusions	37

arXiv:1406.4538v1 [astro-ph.GA] 17 Jun 2014

Abstract

We present an analysis of ~ 13000 stars from RAVE Data Release 4 (DR4) to better understand the formation of the thick disk. The stars we consider are mostly within 1 kpc of the Sun. We used the $[\text{Mg}/\text{Fe}]$ ratio as a guide to the ages of stars and their metallicity ($[\text{Fe}/\text{H}]$) as a guide to their radius of formation. Radial migration was apparent in our dataset and is very helpful observationally.

Based on a Monte-Carlo analysis of the data and comparison with a toy model, we suggest the thick disk formed fairly rapidly when $[\text{Mg}/\text{Fe}] \approx 0.2 - 0.3$. The event which formed it affected the outer regions of our Galaxy more substantially. We consider an origin via direct accretion unlikely as the thick disk is fast-rotating. As internal disk heating is generally more efficient closer to the centre, it also appears implausible.

We suggest the event was an interaction with another galaxy. Tidal interactions would affect the Milky Way more in its outer regions. The data are not suggestive of disk heating over an extended period of time (e.g. due to multiple close passages of another galaxy before it merged). However, distinguishing such a scenario from a single close passage is very difficult at present.

A very early formation of the thick disk (e.g. from star formation in the collapsing primordial gas cloud of the Milky Way) appears unlikely given it would require $[\text{Mg}/\text{Fe}] \geq 0.4$ at the time the thick disk formed. This scenario is possible if the errors in RAVE DR4 were underestimated. However, our data do not show an unphysically large range in $[\text{Mg}/\text{Fe}]$ when allowance is made for the official error budget. Combined with the exhaustive checks done on RAVE data, we believe the error budgets are reasonable.

Our proposed explanation for the nature of the event which formed the thick disk is a close flyby of Andromeda, whose orbital dynamics in MOND are consistent with our estimate that the event occurred 7-11 Gyr ago. This leads to reasonable thick disk velocity dispersions. It will be important to determine whether the event heated the outer regions of the thin disk uniformly or if substantial portions of it were left largely unaffected. This may distinguish between models (like ours) involving a single close encounter and models with multiple encounters. The main limiting factor at present seems to be the accuracy of elemental abundances and lack of direct observations at different galactocentric radii to the Sun.

1 Introduction

Understanding almost any aspect of galaxies will inevitably require fundamental new physics: either an undiscovered particle outside the Standard Model or a substantial modification to our theory of gravity (see e.g. [34] and [35] for why existing physics will be insufficient). Consequently, much may be gained by a better understanding of the formation and evolution of galaxies. Several surveys have been and are conducting detailed observations of galaxies, especially our own. This is the only one with stars close enough that proper motions can realistically be measured at present, allowing a determination of 3D velocities. Despite the proximity of Milky Way stars in cosmic terms, such measurements can still be very difficult and therefore inaccurate. Substantial improvements are expected from ongoing and future surveys, especially the currently operating GAIA mission ([21]).

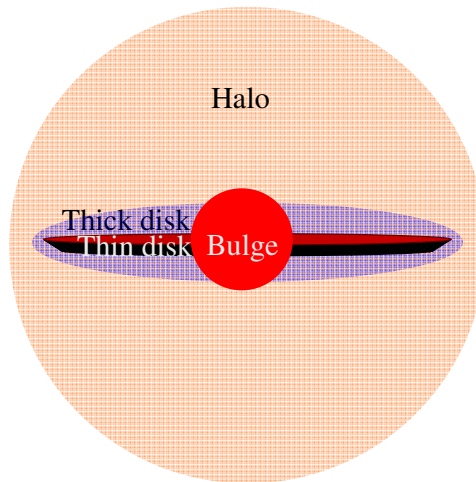


Figure 1: Schematic depiction of the structure of our galaxy. The scale heights of the thin and thick disks are around 300 and 1000 pc, respectively (corresponding to $\sigma_z \approx 20$ and 50 km/s). The scale length of these disks is about 3 kpc. The Sun is in the thin disk, 8 kpc from the centre. The halo also contains orbiting globular clusters and a few satellite galaxies.

The structure of our galaxy is depicted in Figure 1. Although the details are unclear, the thin disk likely formed from dissipative collapse of a slowly rotating gas cloud ([16]). Some of the gas may have been accreted after this initial collapse. Leaving aside the possibility of a dark matter halo (which lacks direct evidence), the vast majority of the mass in our Galaxy is in the thin disk. This is composed of stars and gas, along with small amounts of dust that can greatly hamper our ability to see through it.

The halo is thought to be the remnants of accreted satellite galaxies (this accretion is ongoing - see e.g. [27]). Smaller galaxies tend to be metal poor, perhaps because metals generated in supernovae can escape from these galaxies more easily. Thus, the halo stars are very metal poor. They comprise only a few percent of the Galaxy's mass.

The origin of the thick disk - discovered by Gilmore and Reid in 1983 (see [2]) - remains unclear. It has a much larger scale height than the thin disk and appears to be very old and gas poor. The work of [22] shows the distribution of orbital eccentricities is strongly peaked at low values, making it unlikely to be mostly material accreted from satellite galaxies (as these would generally have fallen in from large radii and so be on highly eccentric orbits).

But heating the thin disk through secular processes such as scattering by giant molecular clouds seems unlikely to lead to the emergence of a kinematically distinct thick disk component with a much larger scale height. Moreover, the work of [23], based on stars with parallax distances from Hipparcos, suggested that disk heating saturates at $\sigma_z \approx 20$ km/s. Although based on a relatively small number of stars, this work identified a sharp rise in σ_z at approximately the correct time to form the thick disk (noting that some of the stars in it may have formed in a pre-existing thin disk and then been heated into the thick disk). They suggested that a minor merger was responsible.

This project was galactic archaeology, the quest to understand conditions in the Milky Way in its first few Gyr of existence. The primary objective was to see if evidence for an ancient interaction with another galaxy exists in the largest currently available survey, RAVE DR4 ([11]).

We discuss the basics of the chemo-dynamical evolution of our galaxy in the remainder of the introduction. This is followed by details of the RAVE survey and our analysis of it, including the galactic co-ordinate system we use. A toy model then investigates whether potential features that may be present in the galaxy could have been detected in this work, given the measurement uncertainties in RAVE data. We then discuss our results in light of this model and other considerations, especially reliability of data. The Appendix gives a simplified model of how the thick disk may have been created during an ancient flyby of Andromeda, which is likely on other grounds. If correct, this would very likely lead to observable consequences, some of which we briefly discuss.

1.1 Constraining Stellar Ages From Distant Observations

The interstellar gas in the Milky Way initially had a very low metallicity. This gradually increased with time, as stars produce heavy elements and enrich the interstellar medium (ISM). Low mass stars can not synthesise some of the heavier elements we study, such as Fe. Thus, their abundance reflects that of the interstellar medium at the time and place the star formed. This information can be obtained billions of years later, from a spectrum. That is primarily what this project seeks to do.

At very early times, the supernovae were mostly core-collapse, with massive progenitors ($M > 8M_{\odot}$). Lower mass stars evolve into white dwarfs, dense objects supported by electron degeneracy pressure. If one has a companion and sufficient material from this is accreted by the white dwarf, it gets close to the Chandrasekhar limit and contracts. This causes it to heat up and fuse the previously inert helium that dominates the white dwarf. The extreme conditions lead to very efficient fusion into iron-peak elements, which have the greatest binding energy per nucleon and so are the most energetically favourable configurations of the available nucleons. This is called a Type Ia supernova, which mostly yields iron.

Magnesium is an α -capture element readily synthesised by core-collapse SNe but not so easily by Type Ia SNe as it does not have the lowest binding energy per nucleon. In the not-so-extreme conditions of non-degenerate heavy stars, the temperatures required to proceed beyond Mg with fusion reactions is only available in the very innermost regions, leading to a shell of Mg which remains inert until the explosion. At that stage, the relatively large size of the star and low density means fusion during the explosion itself often leaves unburnt Mg, which then enriches the ISM.

As lower mass stars survive for longer, there is a delay between the onset of chemical enrichment (core-collapse SNe) and the onset of Type Ia SNe. The relative proportions of heavy elements synthesised by these two types of SNe are different. Consequently, the ratio of elemental abundances in the ISM - and thus in newly forming stars - changes with time (e.g. [3]).

The whole process of chemical enrichment is likely to be faster closer to the galactic centre, where the density of stars is higher. Stars easily migrate to different galactocentric radii in simulations (e.g. [24]). Thus, the metallicity of a star alone can not tell us if it is young and formed at large R (galactocentric radius) or old and formed at small R . The [Mg/Fe] ratio helps to break this degeneracy, because an old star will have been born not so long after the onset of Type Ia SNe. Consequently, these will have reduced the [Mg/Fe] ratio from the value typical of core-collapse SNe by a smaller amount, leading to higher [Mg/Fe].

1.2 Disk Heating & Radial Migration

Most stars in our Galaxy are in the thin and thick disks. The majority of these stars were born in a thin disk of gas. They then gained random velocities through interactions with other stars and giant molecular clouds. Large scale spiral density waves (visible in most disk galaxies) are likely also important in this process of dynamical heating. The rates of such interactions are reduced once stars have gained enough vertical velocities that they no longer spend much time in the thin disk (where most of the possible perturbers are).

Radial velocity dispersion leads to stars in the local solar neighbourhood (LSN) which have both larger and smaller guiding radii for their orbits. However, there are more stars with smaller guiding radii than the Sun, so these will dominate stars in the LSN. Given the nearly flat dependence of the circular rotation velocity on radius ([39]), such stars must have less angular momentum than the Sun and so must be orbiting slower than it. This asymmetric drift effect is more pronounced for populations of stars with larger radial

velocity dispersion, as such stars sample a larger range of galactocentric radii and are thus more affected by the radial gradient in the density of stars.

The orbital radius of a star can be altered substantially while keeping its orbit nearly circular (see [24]). Such radial migration can be driven by large scale spiral density waves, especially near the co-rotation circle (where the angular speed of the spiral pattern equals that of orbiting stars). Here, there is a resonant effect because stars can be affected by the non-axisymmetric potential generated by the spiral wave for a long period of time (the potential appears nearly static to the star). The bar in the central regions of our Galaxy can also cause radial migration, by transferring angular momentum outwards from stars and gas in the central regions (which fall to smaller radii).

Radial migration of this sort only works efficiently for stars that spend a large fraction of their orbit close to the disk plane and also have low σ . High dispersions reduce the amount of time available for torques from e.g. spiral arms to act on the star and alter its orbit before the epicyclic motion of the star takes it far from the spiral arm. For this reason, although the bulge is dynamically hot, it is difficult for such stars to diffuse outwards and raise the velocity dispersion in the solar neighbourhood. These issues are considered in more detail in [25].

2 Methods

2.1 Datasets & Selection Criteria

The Radial Velocity Experiment (RAVE) survey is a magnitude-limited survey of stars in the southern hemisphere conducted using the 1.2m UK Schmidt telescope at Siding Springs National Observatory, Australia ([11]). The survey was conducted at wavelengths $\lambda = 841 - 879.5$ nm and I-band magnitudes of 9 - 12. The survey contains nearly 500,000 stars and its latest data release contains the largest sample of stars to be observed in the same survey. The wavelength range was chosen to include the ionized calcium triplet. More generally, old stars must be fairly low mass and low temperature, making infrared observations better. This also reduces obscuration by dust.

We used proper motions from the fourth United States Naval Observatory CCD Astrograph Catalogue (UCAC4). These had been put in the same file as the RAVE data (proper motions were available for most RAVE stars). This file was saved into a format MATLAB can read (this work was done in MATLAB R2013a). All RAVE data collected before 3rd April, 2004 was deleted because there was a major technical issue by which empty sky was observed instead of the target stars and the calibration lamp essential for measuring radial velocities was also not well set, among other issues. Various filters were then applied to the data. These criteria were designed to be similar to those used in [1], although we got ~ 13000 stars instead of ~ 5000 for unknown reasons (the authors were contacted to find their criteria, but the discrepancy remains unresolved, most likely due to not using *exactly* the same criteria).

The distances were determined in the work of [7]. The metallicity and colour of a star - based on data from the 2MASS survey ([28]) as well as RAVE - are used to determine the likely mass using main-sequence fitting. Then, the surface gravity (which alters the pressure near the star's surface and thus the pressure broadening of spectral lines) is used to determine the size of the star. The effective temperature and size of course determine the absolute magnitude of the star, which is used to determine its distance.

These distances may have systematic errors. Attempts were made to correct for these, based on the effect that distance errors have on the different components of the galactocentric velocity. This effect depends on the star's galactic co-ordinates. Correlations between velocities and galactic co-ordinates are at the heart of the method used ([20]). Distances have been corrected using this technique, which is thought to be valid if the data covers a large fraction of the sky. For our dataset, this condition is satisfied (see Figure 2).

As Figure 3 shows, our sample mostly consists of stars in a sphere 1 kpc in radius centred on Earth, with the height above the disk mid-plane further restricted to 0.6 kpc. We restricted attention to disk stars at galactocentric radii similar to the Sun. This should select thin and thick disk stars but leave little halo contamination. The restriction on $[\text{Fe}/\text{H}]$ is to further reduce halo contamination - halo stars are very metal poor. The restrictions on surface gravity are so we select giant stars. These are at a particular evolutionary stage, making their intrinsic luminosity less dependent on mass. This makes estimates of their distance more accurate. The lower bound on g is because such stars have too little pressure broadening in their spectra for g to be reliably determined.

Parameter	Meaning	Allowed values
eHRV	Error in heliocentric radial velocity	≤ 1.5 km/s
CHISQ_c	How well synthetic spectrum fit actual data	≤ 1000
SNR_K	Signal to noise ratio per pixel	≥ 65
Algo_Conv_K	Convergence of algorithm analysing spectra	0
Teff_K	Surface temperature of star, degrees Kelvin	4000 - 5500
logg_K	$\log_{10}(\text{surface gravity, } cm^2/s)$	0.5 - 3.5
c1, c2, c3	Checking if star binary (see [13])	n
R	Galactocentric radius of star (cylindrical polar system)	7000 - 9000
Z	Perpendicular distance of star to Galactic disk mid-plane	≤ 600
Fe	Abundance of iron, relative to that in Sun	[-1.2, 0.3]

Table 1: Selection criteria used in this work. The last three needed to be applied separately on each Monte-Carlo run (see text) and lead to variations in the sample size between runs.

For the uncertainties on the measured parameters of each star, we usually used the ones listed in the RAVE data release. For [Fe/H], we used the error in the total metallicity (eMet_K). For [Mg/H], we used 0.075 dex independent of the S/N of the stars, because [11] says that it is ≤ 0.15 dex if $S/N \geq 40$ and we used $S/N \geq 65$. Our results were not affected by raising the error in [Mg] to 0.15. Note that there is no allowance for a systematic error due to errors in the solar abundance (obtained from [12]), which all abundances in this work are given relative to. Such an error will affect all values equally, so is of little importance when we are interested in looking for trends.

The error in the ‘parallax’ (distance estimate) was assumed to be logarithmic because it sometimes exceeded 100%. Errors on intrinsic luminosities of stars - used to determine distances - are often given in magnitudes. Thus, we assumed that

$$\Delta(Ln(Parallax)) = Ln\left(1 + \frac{e\text{-parallax}}{parallax}\right) \quad (1)$$

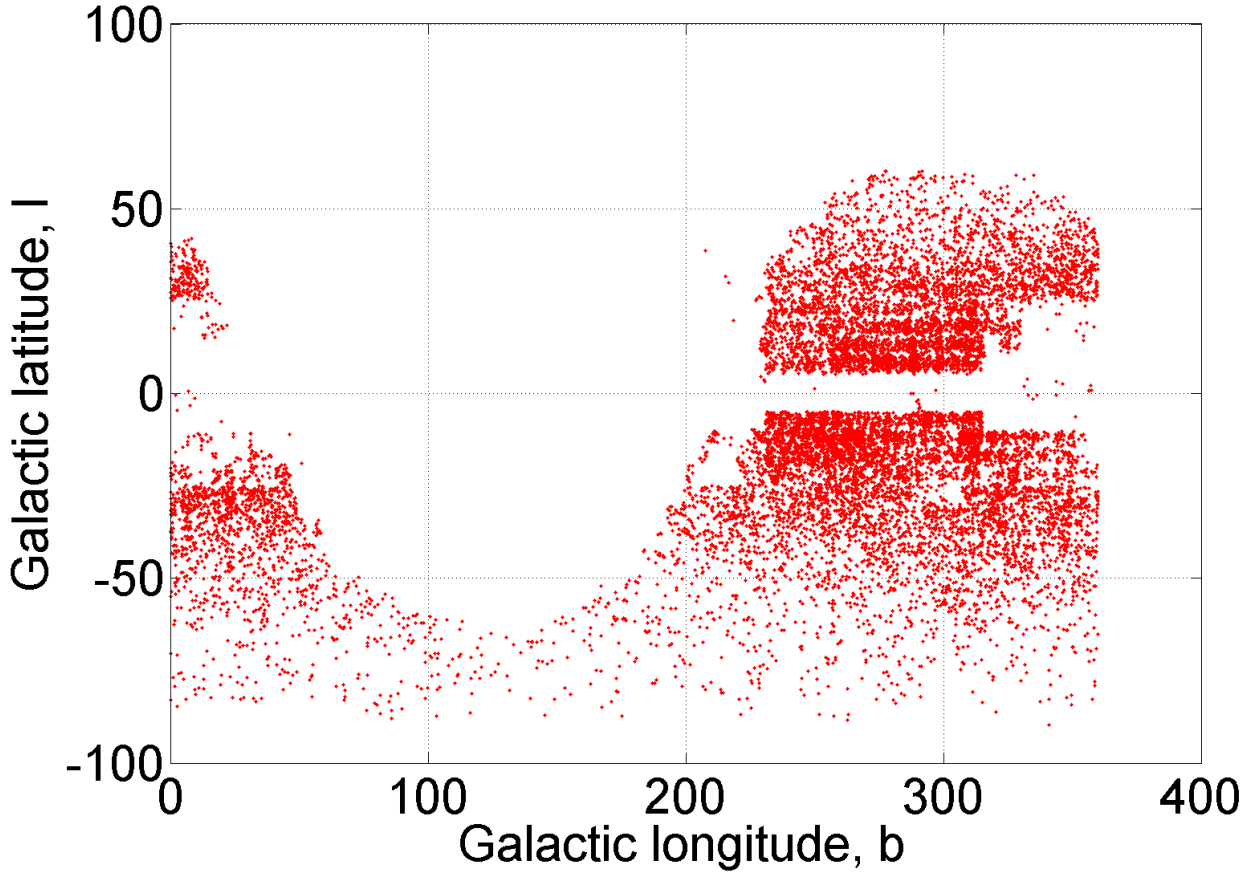


Figure 2: The directions to stars in our sample, in galactic co-ordinates. The galactic disk is along $b = 0$ and $l = 0$ is towards the galactic centre. Note the half of the sky invisible from the observing site and the paucity of observations close to the disk mid-plane.

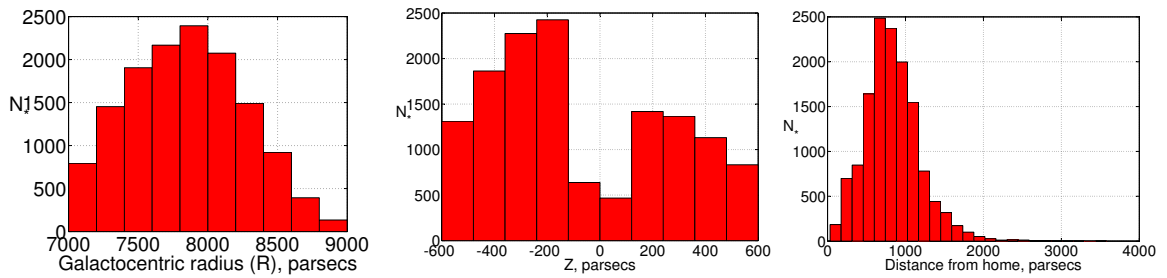


Figure 3: Histograms showing the distributions of galactocentric radii, height above disk mid-plane and heliocentric distances, respectively, of our sample of stars. Dust in the galactic disk makes observations at low $|Z|$ difficult, so only very nearby stars can be observed at low $|Z|$.

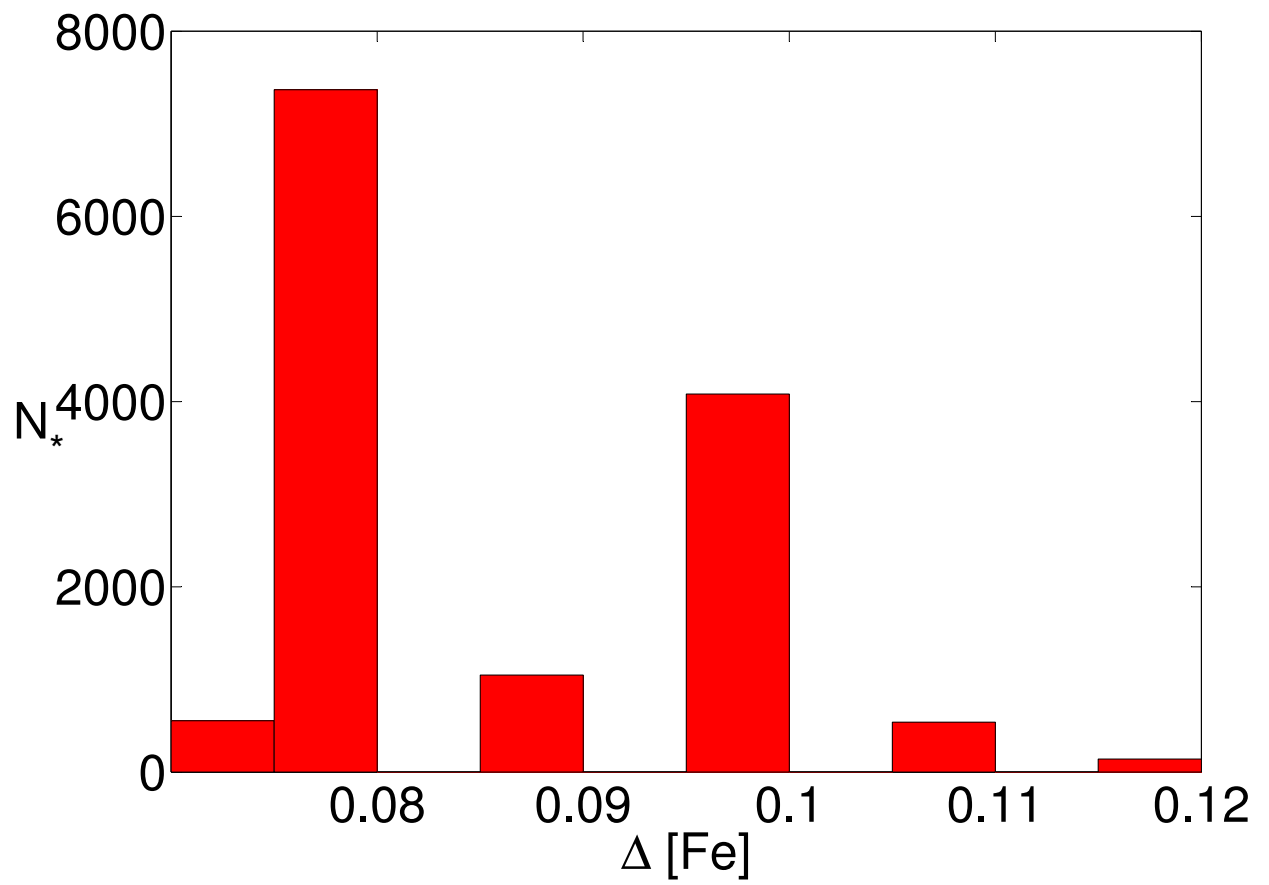


Figure 4: The distribution of the quoted errors in $[\text{Fe}/\text{H}]$ for our sample of stars.

2.2 The Co-Ordinate System

Galactic co-ordinates have much more intrinsic physical meaning compared to celestial ones. The conversion between the co-ordinate systems (where δ and α are celestial co-ordinates and b and l are galactic co-ordinates) is achieved using the following equations:

$$\cos b \cos(l - l_0) = \cos \delta \cos(\alpha - \alpha_N) \quad (2)$$

$$\cos b \sin(l - l_0) = \sin \delta \sin i_G + \cos \delta \sin(\alpha - \alpha_N) \cos i_G \quad (3)$$

$$\sin b = \sin \delta \cos i_G - \cos \delta \sin(\alpha - \alpha_N) \sin i_G \quad (4)$$

Parameter	Meaning	Value
α_N	Longitude of ascending node of galactic plane on Equatorial plane	282.85948°
i_G	Inclination of galactic plane to Equatorial plane	62.87175°
l_0	Galactic longitude of the ascending node just mentioned	32.931924°

Table 2: Parameters of the galactic co-ordinate system used in this work.

Motions of stars are usually referred to the Sun and are written as a μ . For example,

$$\mu_\alpha \equiv \dot{\alpha} \quad (5)$$

Because motions in celestial longitude correspond to less motion on the sky for objects closer to the celestial pole, we multiply all proper motions with respect to longitude of a co-ordinate system by the cosine of the corresponding latitude. In this case, we use a * in the subscript, so e.g.

$$\mu_{\alpha*} \equiv \dot{\alpha} \cos \delta \quad (6)$$

Differentiating the transformation equations with respect to time, we get that

$$\begin{bmatrix} \mu_{l*} \\ \mu_b \end{bmatrix} = \frac{1}{\cos b} \begin{bmatrix} C_1 & C_2 \\ -C_2 & C_1 \end{bmatrix} \begin{bmatrix} \mu_{\alpha*} \\ \mu_\delta \end{bmatrix} \quad (7)$$

$$C_1 = \cos i_G \cos \delta + \sin i_G \sin \delta \sin(\alpha - \alpha_N) \quad (8)$$

$$C_2 = \sin i_G \cos(\alpha - \alpha_N) \quad (9)$$

The conversion of heliocentric velocities into galactocentric ones is effected by means of a Galilean transformation, followed by another change of co-ordinates. This has been done in the appendix of [6]. The solar position and velocity used for this report are listed in Table 3.

Parameter	Value
R_\odot	8000 pc
U_\odot	11.1 km/s
V_\odot	12.24 km/s
W_\odot	7.25 km/s
$v_{c,0}$	226.84 km/s

Table 3: Position and velocity of the Sun with respect to the galaxy, obtained from [18]. Parameter meanings as in [6]. U is positive towards the galactic centre, V is tangential to this and within the disk plane in the direction of rotation while W is positive towards the North Galactic Pole.

2.3 Monte-Carlo Procedure & Binning The Data

Depending on what we were doing, up to 6 input parameters were varied using a Monte-Carlo procedure, to get a good idea of what the outcome of our analysis would have been had the actual stellar parameters been slightly different to the measurements (but within their uncertainties). These were the two proper motions, radial velocity, downrange distance and abundances of Fe and Mg. The error budgets used were described previously. As we were unsure about the error in $[\text{Mg}/\text{H}]$, we doubled it but found the results hardly changed.

The standard random number generator of MATLAB R2013a was used, each time to generate just a single random number. This gives a number randomly distributed between 0 and 1. To generate a random variable with a Gaussian distribution, we then determined the value of x such that

$$\frac{1}{\sqrt{2\pi}} \int_{-\infty}^x e^{-\frac{x^2}{2}} dx = rand \quad (10)$$

This was achieved using the `erfinv` function. This procedure was always performed before generating another random number and makes the computer unlikely to be influenced by previous runs of the random number generator.

We developed a binning algorithm with fixed bin widths in parameters such as $[\text{Fe}/\text{H}]$. If there were too few stars in the bin for our liking, we merged adjacent bins (usually to get $N \geq 80$). Rerunning the analysis on mock data would inevitably shift the positions of the bins, so we decided to run the algorithm once (with all inputs set to their measured values) to see which values of e.g. $[\text{Fe}/\text{H}]$ the bins should be at. In the subsequent analysis, the bins were kept fixed at these positions so Monte-Carlo runs could sensibly be compared with each other.

An important feature of our code is that stars can move between bins or fall outside the selection criteria as their input parameters change. This meant that there was no way to guarantee what the number of stars in each bin would be. We supposed that, given 80 or more stars in each bin when input parameters equal their measurements, there would always be enough. In fact, the number of stars in each bin hardly varied between runs.

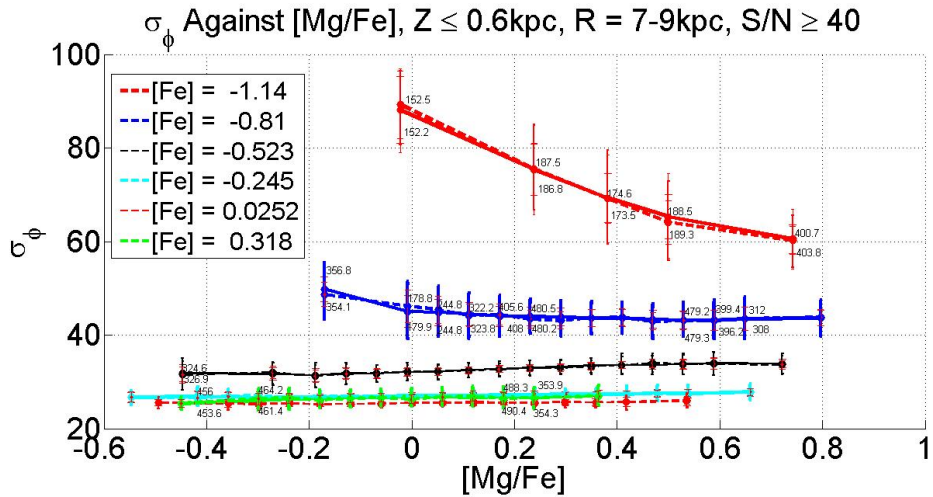


Figure 5: Results for the tangential velocity dispersion, with data binned by both $[\text{Fe}/\text{H}]$ and $[\text{Mg}/\text{Fe}]$. The dashed lines show the results for 100 Monte-Carlo runs while the solid line shows the results for 500 runs (not including the first 100). The numbers indicate the mean number of stars in each bin, if this is below 500.

We checked if we had performed enough Monte-Carlo realisations to achieve convergence of the outcome. The usual procedure was to do 500 runs because our results indicated there was not much difference once at least 100 runs had been performed (see Figure 5).

2.4 Parameter Extraction & Error Budgets

The parameters that we extracted for each bin were mean chemical abundances, velocity dispersions & mean values and the number of stars assigned to the bin. The velocity dispersion was simply the standard deviation of individual stellar velocities and mean values were unweighted. However, we rejected all stars with galactocentric speeds exceeding 1000 km/s as this greatly exceeds the escape speed from the Milky Way ([31]).

For each bin, the best-fit value of any parameter was taken to be the mean over a large number of Monte-Carlo runs. The error budget was allowed to be asymmetric and involved finding the parameter value such that 84.13% of the runs returned values which were even higher (or lower), giving a 1σ error bar. However, this procedure sometimes misses important contributions to the uncertainty.

The most important such case was the finite sample effect for velocity dispersions. It is fundamentally impossible to get a fractional accuracy in velocity dispersion better than $\frac{1}{\sqrt{2N}}$ from observations of N stars, even if these stars were perfectly measured. In that case, the Monte-Carlo procedure would give a zero error budget. Thus, we added $\frac{\sigma}{\sqrt{2N}}$ in quadrature to the uncertainty suggested by the Monte-Carlo procedure.

When determining the number of stars assigned to a particular bin, there is a similar effect called Poisson noise. The fundamental limit in fractional accuracy is $\frac{1}{\sqrt{N}}$. This is absent in a Monte-Carlo analysis and was therefore added in quadrature. There was a similar effect when estimating the mean velocity of a sample of stars, for which the minimum uncertainty is $\frac{\sigma}{\sqrt{N}}$, where σ is the best estimate of the velocity dispersion in that direction.

2.4.1 Dangers Of Small Sample Sizes

One shortcoming of the analysis used in ([1]) is the small number of stars in the [Mg/Fe] bins that supposedly show unusually low velocity dispersions (see Figure 19). Suppose the velocities of the 11 stars in the highest [Mg/Fe] bin are known exactly and that the chemical abundances of these stars are also known exactly such that they can be unambiguously assigned to this bin. Then, there are only 10 effective degrees of freedom when calculating σ .

Assume there are a large number of stars in the same range of [Mg/Fe] as that bin (and satisfying the other selection criteria) in our Galaxy. Suppose these stars have a Gaussian distribution of velocities. A random sample drawn from this will have *on average* a squared deviation from the mean value equal to the true dispersion, σ . Let

$$\chi^2 \equiv \sum_{i=1}^{N_*} \left(\frac{v_i - \bar{v}}{\sigma} \right)^2 \quad (11)$$

\bar{v} is the mean velocity of the sample and the sum includes all stars in it. σ is unknown a priori. Usually, it is assumed that $\chi^2 = N_* - 1$ and σ is solved for. The probability distribution of χ^2 for 10 dof is shown in Figure 6.

The most likely value of χ^2 is actually 8, so our estimate of σ may be biased. As $\sigma \propto \frac{1}{\sqrt{\chi^2}}$, we simply need to determine $E\left(\frac{1}{\sqrt{\chi^2}}\right)$ and compare with $\frac{1}{\sqrt{10}}$. As Figure 6 shows, lower values of χ^2 and so higher values of σ are going to result. In this case, the calculation suggests we should raise σ by 9% to account for skew in the χ^2 distribution. This arises because, with a small number of stars, the tails of the Gaussian distribution may not get sampled at all.

This effect is larger when the velocity dispersion is dominated by the high velocity tail of a high-dispersion subpopulation within the sample, as it is the number of stars belonging to that subpopulation rather than the total number which really matters. In Figure 19, the rise in σ with [Mg/Fe] is due to an increasing fraction of thick disk stars. These may comprise most of the stars in high [Mg/Fe] bins, but there are probably some thin disk stars (with low σ) in these bins too. Therefore, with even less than 11 thick disk stars, it would not be too surprising if the velocity dispersion in the highest [Mg/Fe] bin was underestimated.

Another feature obvious from Figure 6 is that substantially different values of χ^2 are plausible. At a 95% confidence level, assuming a single population with Gaussian distributed velocities, the true value could be

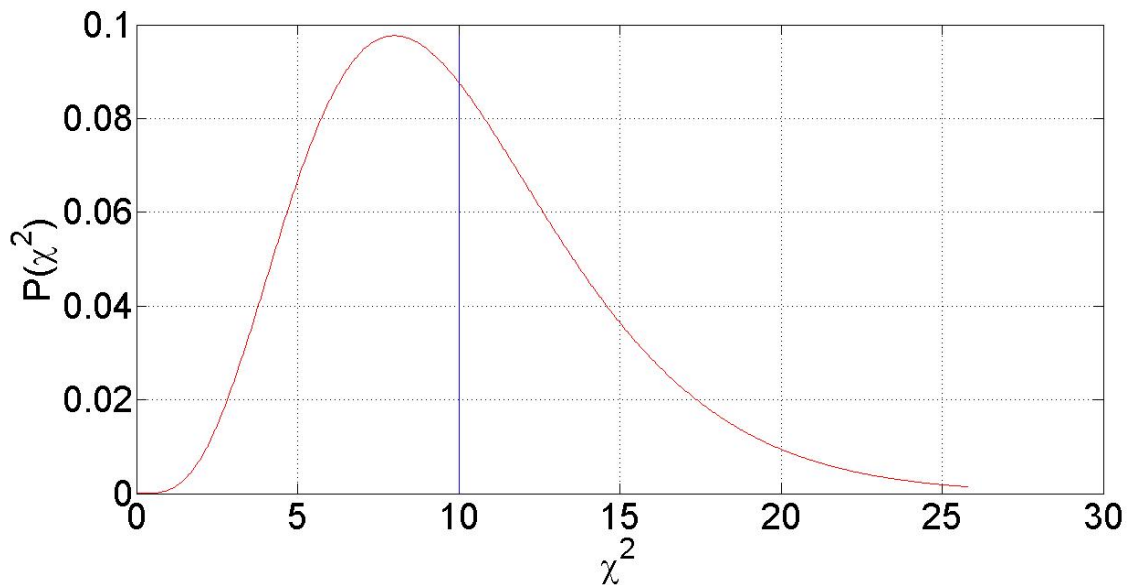


Figure 6: The χ^2 probability distribution for 10 degrees of freedom is shown. Note the distribution peaks at less than 10 (vertical line), although this is the mean value.

3-21. This means σ could be 80% higher or 30% lower than if $\chi^2 = 10$. This shows that an (uncorrected) velocity dispersion estimate of 30 km/s is consistent with a true value of 54 km/s, even without considering any sort of measurement error.

Similarly, with 11 stars and a velocity dispersion of about 40 km/s, the mean velocity of the sample can't be determined to better than an accuracy of $\frac{\sigma}{\sqrt{N}}$. A reasonable null hypothesis might be that σ and $\langle v_\phi \rangle$ stayed the same between the two highest [Mg/Fe] bins. The statistical significance of the observed drop in asymmetric drift when going from the second highest to the highest [Mg/Fe] bin would therefore appear low.

So far, we ignored measurement errors. If, in the work of [1], the number of stars in each [Mg/Fe] bin was allowed to vary between Monte-Carlo runs (like in our analysis) then some of the Monte-Carlo runs would have even less than 11 stars in a bin (and even less thick disk stars). We suggest that, as it is known small numbers of stars tend to depress their measured velocity dispersion, the sharp drop in σ with [Mg/Fe] is due to a steep decrease in the number of stars in these bins.

The high importance of distance errors in determining velocities leads to correlations amongst the measured velocity dispersions in the three spatial directions. This means that, if an unusual feature in velocity dispersion data appears in one component, it is likely to appear in other components as well (because it may be a problem with distances). Also, if a bin has no thick disk stars, all three velocity dispersions and the asymmetric drift will appear small. Consequently, measurements of the three velocity dispersions are not independent, as they rely on the same stars.

The best-fit distances may be biased, especially considering that [11] highlighted an issue with metal-poor giant stars such as those crucial to the work of [1]. Various priors had to be put on stellar parameters to obtain the distances used in that study. With a small sample, even one star with erroneous distance can matter a lot. Given all the uncertainties highlighted, it seems reasonable to conclude that there was no statistically significant detection of a reduction in velocity dispersion with increasing [Mg/Fe] in the work of [1].

3 Results

We begin by showing the relation between $[\text{Mg}/\text{Fe}]$ and $[\text{Fe}/\text{H}]$ of our sample (Figure 7), to see if there is evidence of any sharp increase in the star formation rate that may have caused a bump in the graph. There is no strong evidence for this, though the next section suggests such features may be hidden by observational errors.

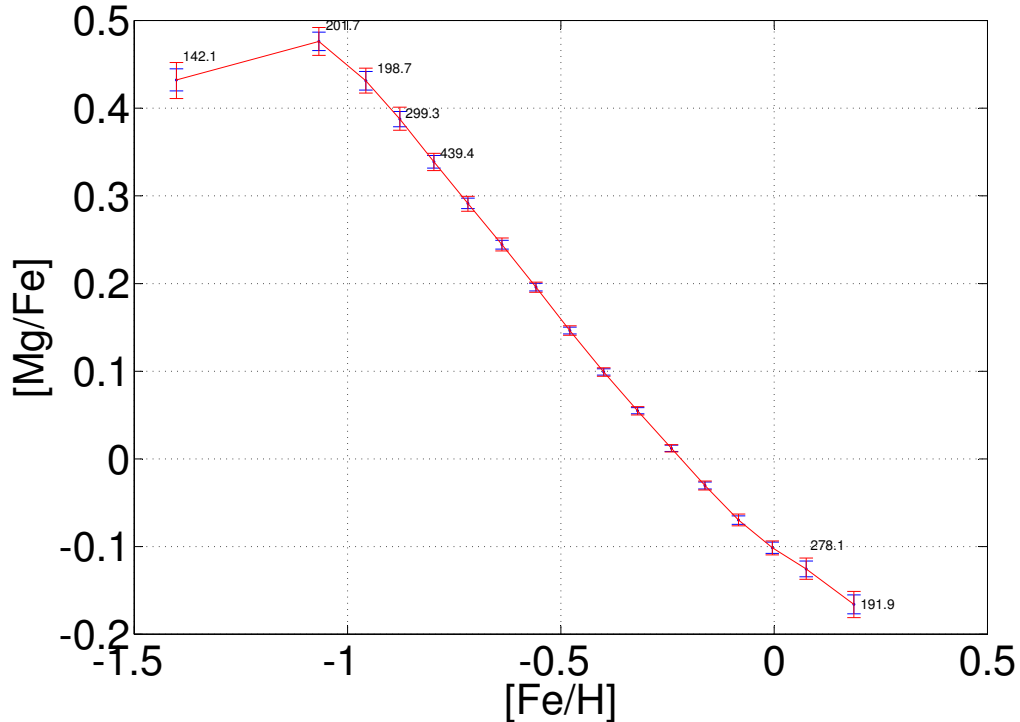


Figure 7: The relation between $[\text{Mg}/\text{Fe}]$ and $[\text{Fe}/\text{H}]$ for our sample. The interior error budget is a guide to the maximum likely contribution from Mg, so we plotted $\frac{0.15}{\sqrt{N}}$. \bar{N} is the mean number of stars in the bin, which is displayed unless it exceeds 500. There is very little error in the mean metallicity of the stars in each bin. This will also be true for $[\text{Mg}/\text{Fe}]$ in subsequent graphs.

There is a fairly substantial spread in the $[\text{Mg}/\text{Fe}]$ values of stars assigned to any given bin in $[\text{Fe}/\text{H}]$. We attribute the majority of this to observational errors, though there will be a small intrinsic dispersion. Figure 8 shows the distribution of $[\text{Mg}/\text{Fe}]$ values for the whole sample. We suggest the two most extreme bins correspond to unphysical values of $[\text{Mg}/\text{Fe}]$, with the increase in number perhaps caused by the fact they are infinitely wide, unlike other bins.

The velocity dispersions and asymmetric drift are shown in the remaining figures in this section. At low velocity dispersions, we should get

$$\frac{\sigma_\phi}{\sigma_R} = \frac{\kappa}{2\Omega} \quad (12)$$

κ is the frequency of small radial oscillations and Ω is the mean angular speed. By determining the Oort constants (which measure differential rotation in the galaxy and thus the shape of the rotation curve), it is known $\kappa \approx 1.4\Omega$ (see [39]). The value we obtain for $\frac{\sigma_\phi}{\sigma_R}$ is consistent with this, suggesting little inflation in velocity dispersions by *random* measurement errors.

In Figure 16, we relaxed the restriction on $[\text{Fe}/\text{H}]$. This led to a large number of halo stars contaminating the lowest metallicity bin. If the nearly spherical halo is assumed to have a scale height of 8 kpc at the solar radius and contain 5% of all the stars in the Galaxy, then only $\sim 0.4\%$ of stars in our sample should be halo stars, corresponding to ~ 50 . As the lowest metallicity bin contains ~ 140 stars and the very high dispersion

$Z \leq 0.6\text{kpc}$, $R = 7\text{-}9\text{kpc}$, $S/N \geq 60$, 500 Runs, $\Delta \text{Mg} = 0.075$

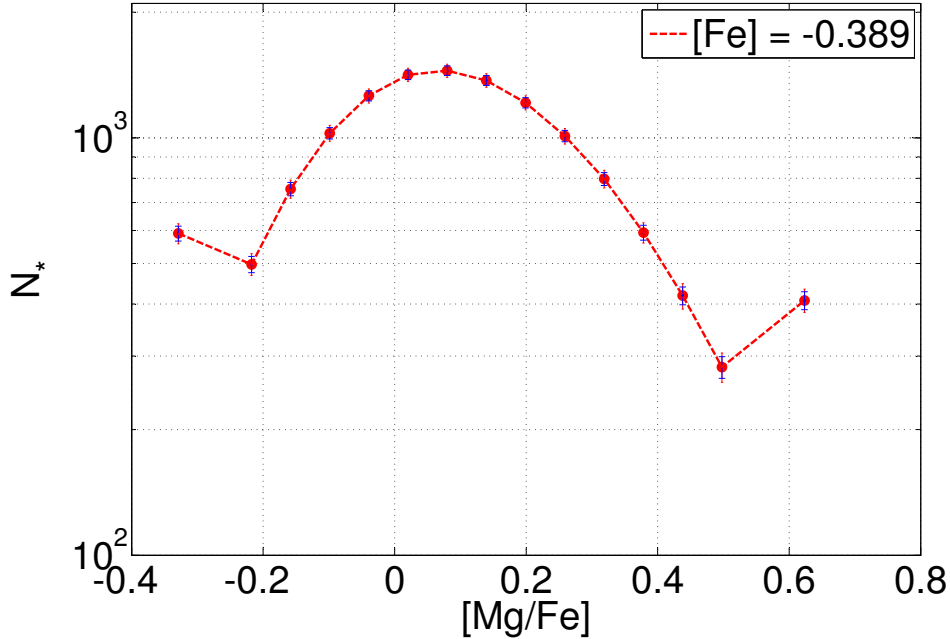


Figure 8: The distribution of $[\text{Mg}/\text{Fe}]$ values in our sample. The error budgets include a contribution from Poisson noise (\sqrt{N}) - this dominates. The legend shows the mean $[\text{Fe}/\text{H}]$ of the entire sample. Note the actual range of values is smaller due to measurement errors (as a guide, the two most extreme bins have unphysical $[\text{Mg}/\text{Fe}]$).

is likely a sign of substantial halo contamination, we suggest that most halo stars in our sample are in that bin. As other graphs were based on data which excluded stars at such low metallicities (minimum of -1.2 dex imposed), halo contamination should not much affect them.

The results in Figures 9 - 11 have stars with similar $[\text{Mg}/\text{Fe}]$ (and thus ages) but different $[\text{Fe}/\text{H}]$. There is little cross-contamination between metallicity subpopulations as $\Delta Fe \approx 0.1$. Thus, we take this result to be a sign of radial migration. The higher density of stars at lower R makes the metal enrichment process faster. The results suggest stars born in the solar neighbourhood with $[\text{Mg}/\text{Fe}] \geq 0.1$ have thick disk velocity dispersions, while stars born closer in have thin disk/ intermediate σ .

The thick disk appears to have been formed at $[\text{Mg}/\text{Fe}] \approx 0.25$, assuming independent errors in $[\text{Mg}]$ and $[\text{Fe}]$ of ~ 0.1 (or that the error in $[\text{Mg}]$ dominates and is ~ 0.15). This is based on adding $\sqrt{2}$ times the measurement error in $[\text{Mg}/\text{Fe}]$ to the lowest $[\text{Mg}/\text{Fe}]$ value in the lowest metallicity subsample (note both measurement errors and the Monte-Carlo procedure increase the apparent range of data, hence the $\sqrt{2}$). It appears unlikely, given that Figure 7 shows $[\text{Mg}/\text{Fe}] \approx 0.45$ at the earliest times, that the thick disk is a relic of the very earliest stages of the formation of our Galaxy (e.g. due to star formation while the primordial gas cloud of the Milky Way was collapsing). The dynamical timescale for the Milky Way is a few hundred Myr, much less than that for Type Ia SNe to cause $[\text{Mg}/\text{Fe}]$ to start decreasing. Thus, we assume the thin disk was well established when $[\text{Mg}/\text{Fe}] = 0.3$. As the thick disk is fast-rotating (see Figures 12 and 14 and also the work of [22]), we consider accretion unlikely. For its age, the rather high metallicity (≈ -1.2) also argues against accretion of gas subsequent to the formation of our Galaxy. Instead, it appears that the thick disk formed from dynamical heating of a pre-existing thin disk which had undergone chemical enrichment.

There seems to be a clear correlation between how much stars were affected by the thick disk creation event and their birth radius, with lower metallicity (higher R_{birth}) stars being more affected. This is a little unusual, as the higher density at lower R suggests there are more objects which may perturb a star there, so stars born at lower R should have higher dispersions (unless the heating occurs differently).

Migration of stars - so crucial to our work - relies upon interactions between stars with the disk. Thus,

it is inefficient for stars with sufficiently high velocity dispersion. The highest two metallicity subsamples suggest the process is inefficient above $\sigma_Z = 30$ km/s. Thus, one could argue that the velocity dispersions were raised everywhere to about 50 km/s but inhomogeneously so some dynamically cold stars remained and these migrated. This scenario is similar to what we suggest in Section 6.1.

Although this may argue against the heating event being more efficient at larger R , it also argues against internal disk heating above 30 km/s, because this relies on interactions between stars and the disk. If, for a given star, these interactions can not cause migration because they are too rare, it is dubious that they can raise its velocity dispersion. Moreover, theoretical arguments suggest such processes can not operate much above 30 km/s (e.g. [25]).

Figure 14 illustrates the difficulty of matching the observed pattern of asymmetric drift for these stars without some sort of rapid heating event. Stars born recently would have a higher metallicity and therefore end up in higher metallicity subsamples. Given that all of these subsamples have no asymmetric drift at sufficiently low $[\text{Mg}/\text{Fe}]$ - which is what one would expect - it seems clear that the stars born at the greatest galactocentric radii must have been heated fairly rapidly at some point.

Stars with $[\text{Mg}/\text{Fe}] \geq 0.45$ were born so early they would most likely end up in the lowest metallicity subpopulation in Figures 9 - 11. This is suggested by the data for higher metallicity subsamples not reaching such high $[\text{Mg}/\text{Fe}]$ values (see Figure 15) despite such subsamples having more stars (see Figure 18). However, this is not true at $[\text{Mg}/\text{Fe}] = 0.2$, so if the thick disk was in place then, we might expect the low metallicity subsample in Figure 11 to have higher dispersion here and lower at 0.4, where some stars born at low R may be contaminating it and depressing σ .

This does not seem to happen. We suggest the oldest stars migrated into the LSN before the thick disk was created (and so ended up with high σ). Stars born at low R shortly before the event would likely not show up in the lowest metallicity subsample: Figure 15 shows that the second-lowest subsample extends to $[\text{Mg}/\text{Fe}] > 0.2$, so such stars would end up in this subsample (or even metal-richer ones). This is especially true if star formation started earlier in the dense inner regions of our Galaxy, as a particular $[\text{Mg}/\text{Fe}]$ value would then correspond to earlier times for stars born at lower R (making it more likely they migrate into the LSN before the event).

Stars born in the LSN before the event end up in the lowest metallicity subsample in Figures 9 - 11 at $[\text{Mg}/\text{Fe}] \approx 0.2 - 0.45$, the slightly wider range in these graphs being due to measurement errors. A few stars born in the LSN shortly before the event might be sufficiently metal-rich to enter the second-highest metallicity subsample. However, these subsamples would likely be dominated by stars born at lower R which later migrated, as suggested by Figure 15.

It seems likely the oldest stars would mostly be in the thick disk, something suggested by Figures 13 and 14. Stars born in the LSN after the event would likely end up in high-metallicity subsamples at low $[\text{Mg}/\text{Fe}]$. Forming in the thin disk after the event, they should have low σ . This appears consistent with the data in Figures 9 - 11. Metal-poor stars - likely old and born at large R - should be in the thick disk and thus have a high velocity dispersion and asymmetric drift. The results in Figures 16 and 17 show this is correct.

For completeness, we also reproduce the results of [1] for velocity dispersions, when sorting stars in both $[\text{Mg}/\text{Fe}]$ and $[\text{Fe}/\text{H}]$. This is shown in Figure 19. However, we do not consider these results reliable due to the low number of stars in crucial bins.

We varied most of the selection criteria (one at a time) to see if our results were very sensitive to them. These analyses were compared with an analysis that did not impose the restriction on surface gravity and allowed radial velocity errors up to 5 km/s, as well as relaxing a few other things (especially allowing `Algo_Conv_K` to be 0 or 2). This was because the selection criteria used for the results just presented could not, in our opinion, be further tightened while still leaving sufficiently many stars to reliably analyse their properties.

The effect of allowing `Algo_Conv_K` to be 0 or 2 was minimal, but we believe the $\sim 20\%$ increase in sample size makes this a good idea. Tightening the restriction on `CHISQ_c` from 1050 to 800 had little effect, but lost $\sim \frac{1}{3}$ of the stars. Relaxing the restriction on $|Z|$ to 1 kpc slightly raised all velocity dispersions, but very little. Relaxing the restriction on R to 6.5-9.5 kpc had little effect. Raising the error in $[\text{Mg}]$ to 0.15 dex had little effect. Relaxing the requirement on the signal to noise ratio per pixel to 40 widened the extent of the data in $[\text{Mg}/\text{Fe}]$ but did not much alter the velocity dispersions. It should be feasible to maintain the quality of data used in this work while relaxing some of the selection criteria, but allowing stars with lower S/N spectra appears to be a bad idea.

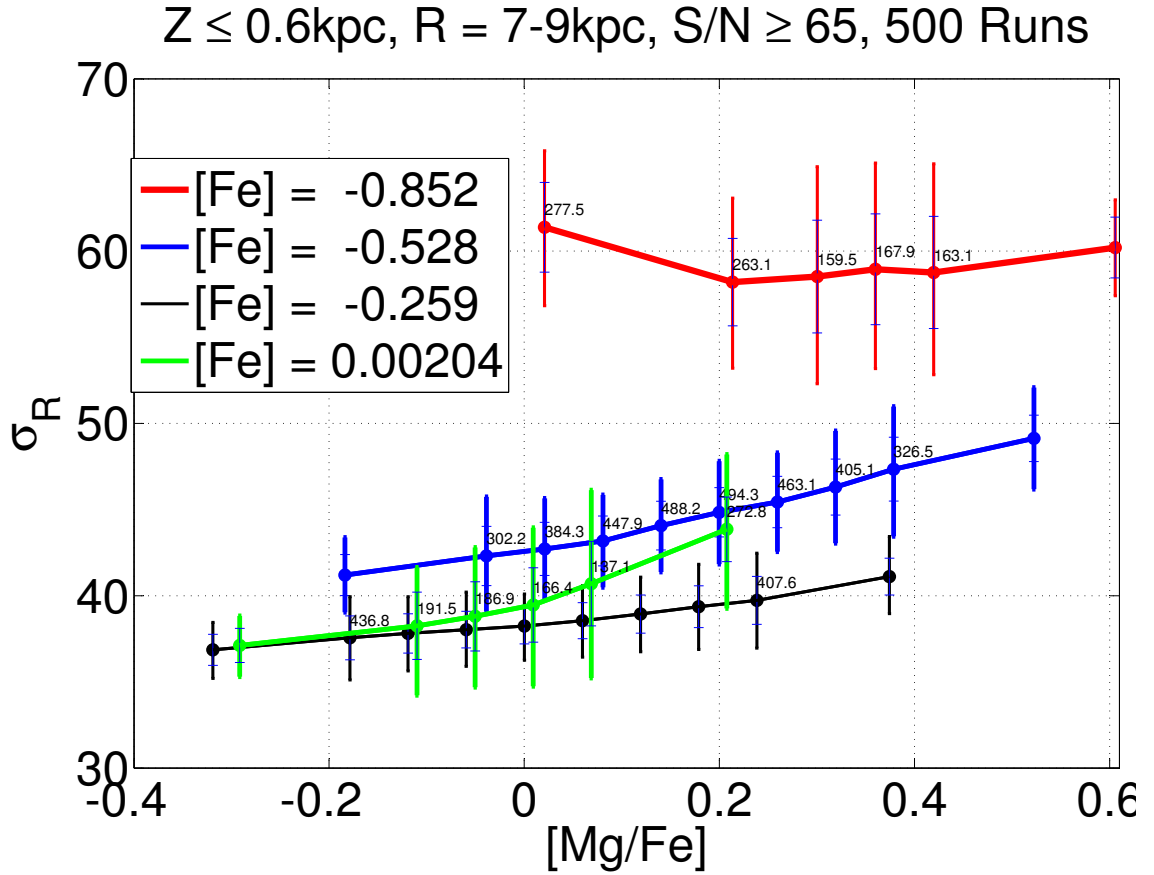


Figure 9: The radial velocity dispersion of our sample, sorted in both $[\text{Mg}/\text{Fe}]$ and $[\text{Fe}/\text{H}]$. The legend indicates the mean $[\text{Fe}/\text{H}]$ for each series (points connected by a line). The error budgets include a contribution due to the finite number of stars ($\frac{\sigma}{\sqrt{N}}$), which is shown as the inner error budget. This was added in quadrature. Note the relatively large differences in $[\text{Fe}/\text{H}]$ between the subpopulations - this makes it unlikely stars will end up in the wrong subpopulation due to measurement errors of $\Delta Fe \approx 0.1$.

We also analysed the data without performing a Monte-Carlo analysis, to see if the velocity dispersions were inflated by measurement errors. If all stars had the same velocity and the measurement error was 10 km/s, the dispersion would be 10 km/s in such an analysis but would rise to 14.1 km/s in a Monte-Carlo analysis because, on average, the mock velocities used in it differ even more from the true value. However, we found no substantial increase in σ due to the Monte-Carlo procedure (it even reduced σ sometimes). This was true even for bins with low velocity dispersions (we sorted the data in $[\text{Fe}/\text{H}]$ only for this test). This suggests the velocity dispersions we found are mostly intrinsic and not due to measurement errors.

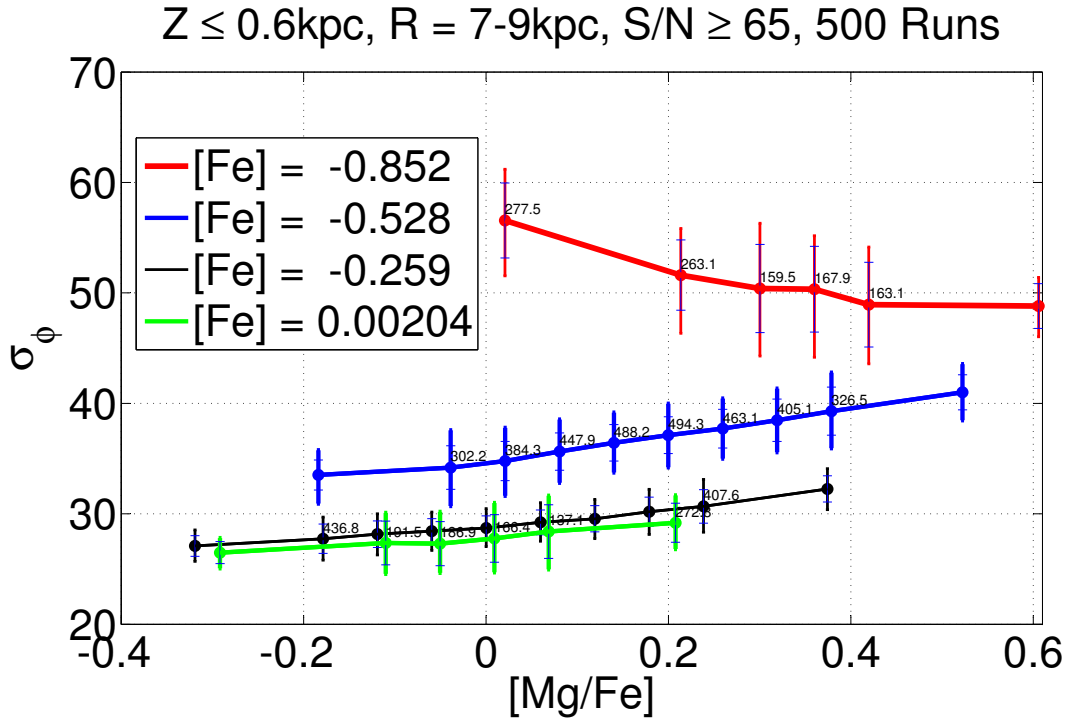


Figure 10: The tangential velocity dispersion of our sample, sorted in both $[\text{Mg}/\text{Fe}]$ and $[\text{Fe}/\text{H}]$.

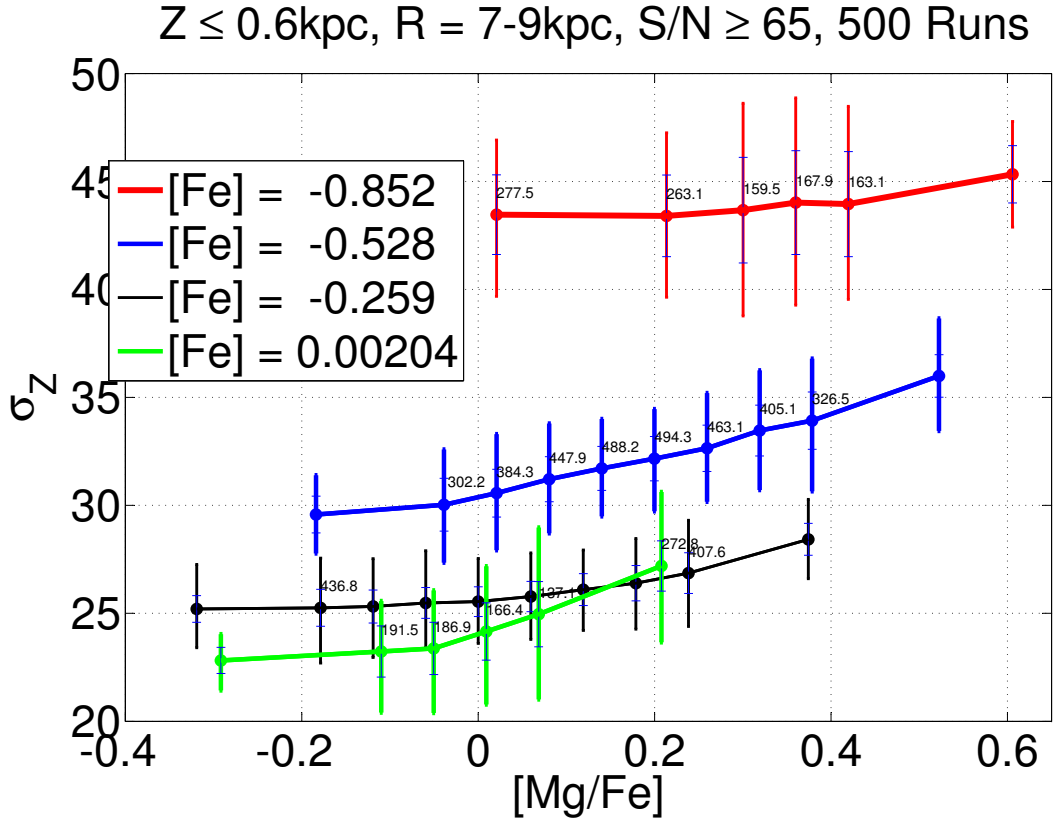


Figure 11: The vertical velocity dispersion of our sample, sorted in both $[\text{Mg}/\text{Fe}]$ and $[\text{Fe}/\text{H}]$.

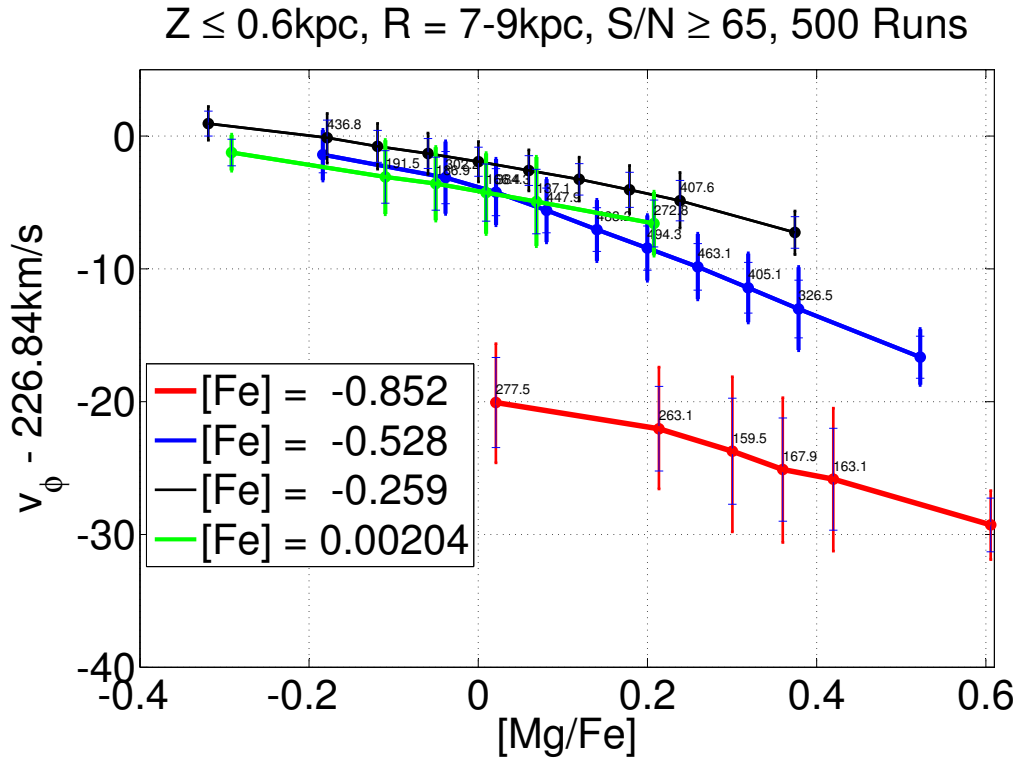


Figure 12: The asymmetric drift of our sample. The inner error budget shows $\frac{\sigma}{\sqrt{N}}$, the fundamental limit to the accuracy of \bar{v}_ϕ . This was added in quadrature.

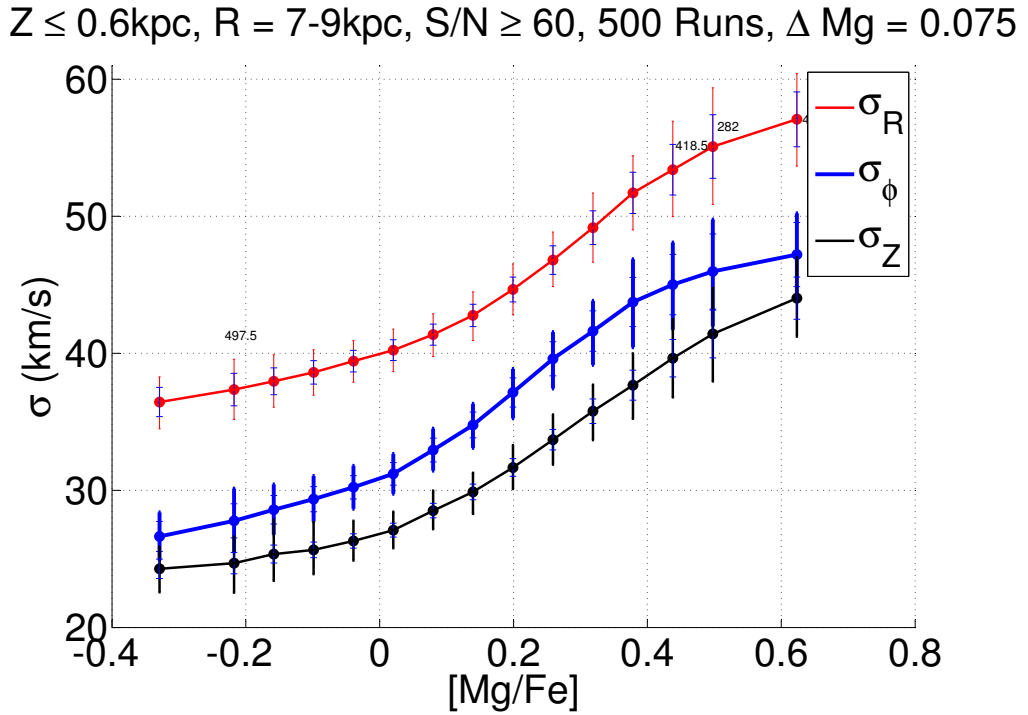


Figure 13: The velocity dispersion of our sample, with sorting only in $[\text{Mg}/\text{Fe}]$.

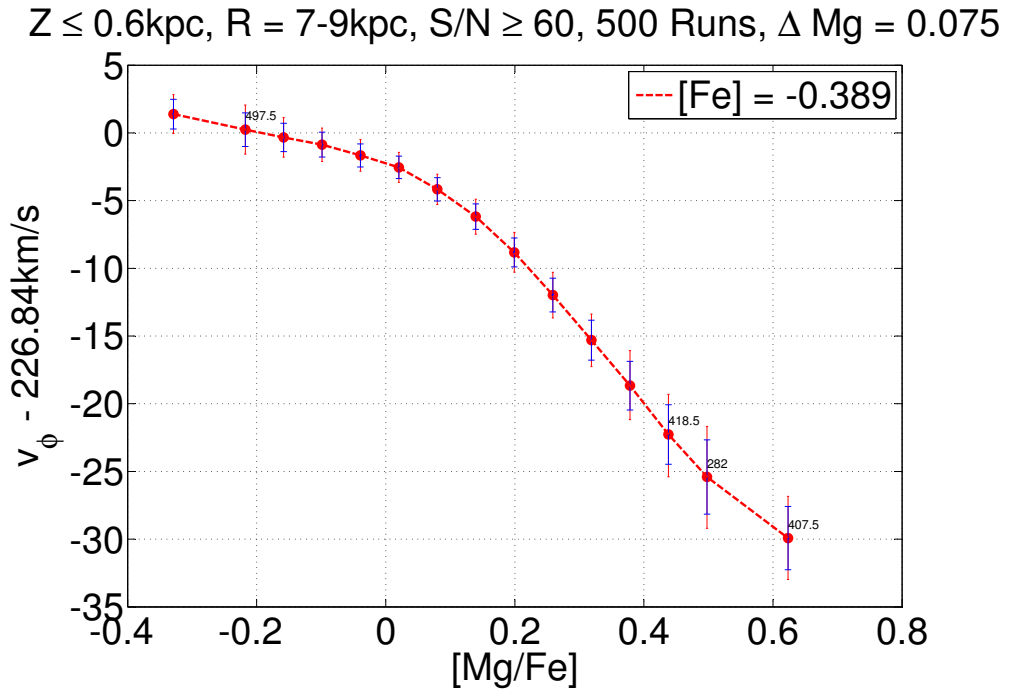


Figure 14: The asymmetric drift of our sample, with sorting only in $[\text{Mg}/\text{Fe}]$. The legend shows the mean $[\text{Fe}/\text{H}]$ of the entire sample.

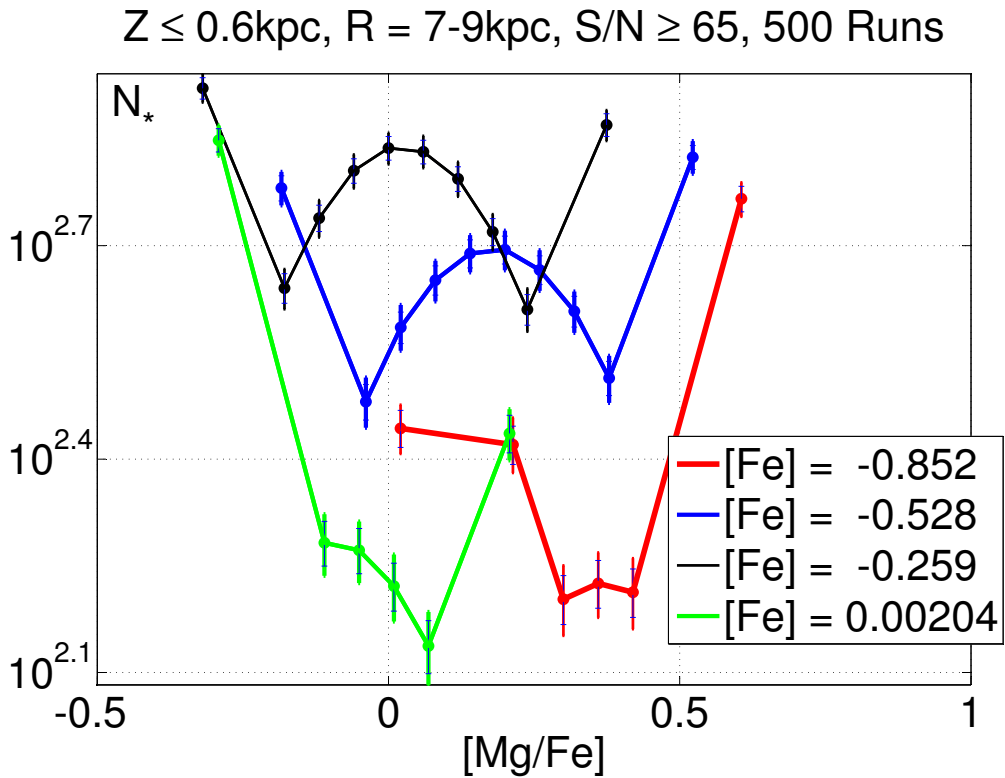


Figure 15: The distribution of $[\text{Mg}/\text{Fe}]$ values for stars in our sample. The uncertainty shown is mostly Poisson noise (inner error bars), which we added separately to the variation between Monte-Carlo runs. As a guide, the two most extreme $[\text{Mg}/\text{Fe}]$ values in each series are unphysical and due to measurement errors.

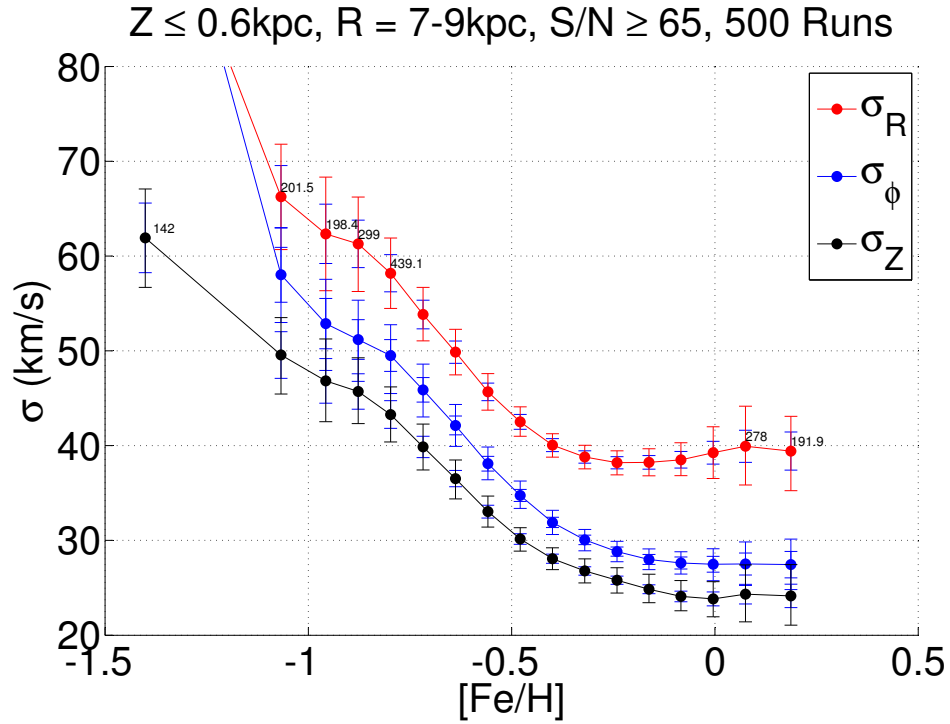


Figure 16: The velocity dispersion of our sample, with sorting only in $[\text{Fe}/\text{H}]$. We relaxed the criterion of $[\text{Fe}/\text{H}] > -1.2$. For clarity, two data points are not shown - they are at $\sigma_R \approx \sigma_\phi \approx 110 \pm 10$ km/s. Note the lowest metallicity bin has σ_Z reduced by selection effects: the data were restricted to low $|Z|$, preferentially selecting stars on orbits not much inclined to the disk plane.

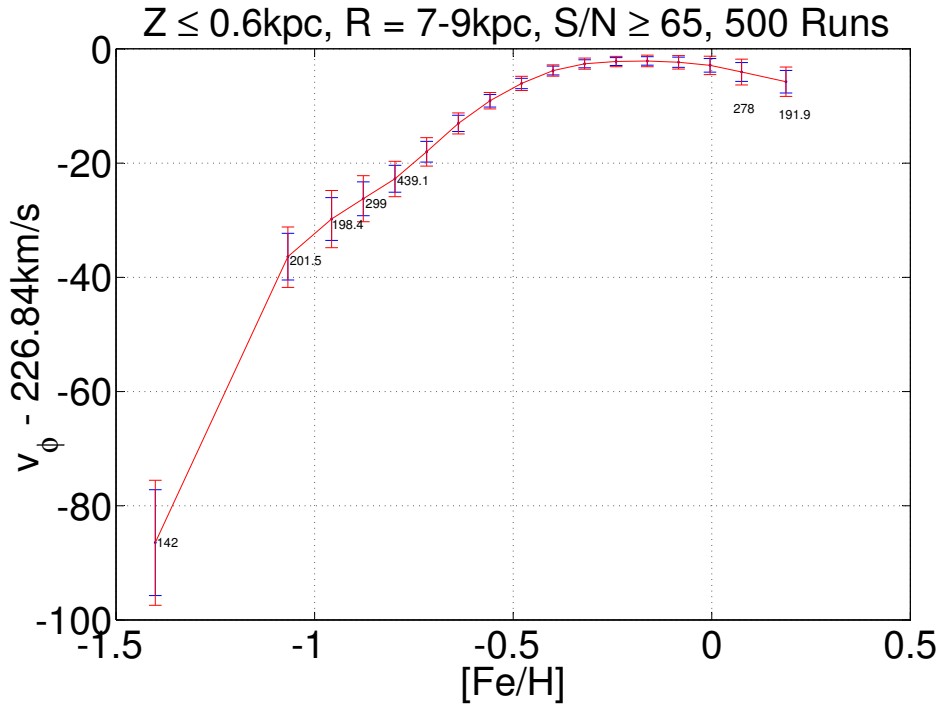


Figure 17: The asymmetric drift of our sample, with sorting in $[\text{Fe}/\text{H}]$ only.

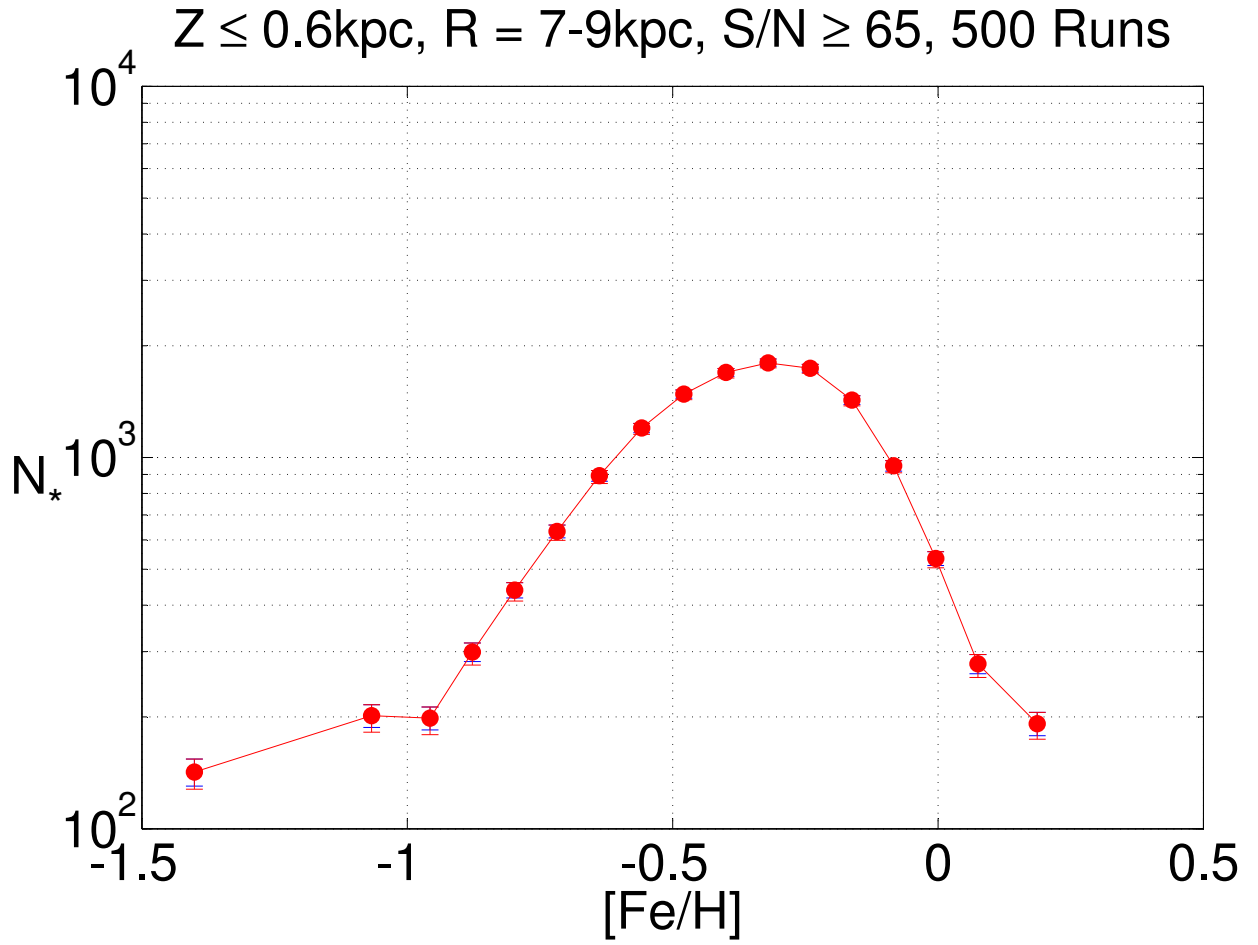


Figure 18: The distribution of $[\text{Fe}/\text{H}]$ values for stars in our sample.

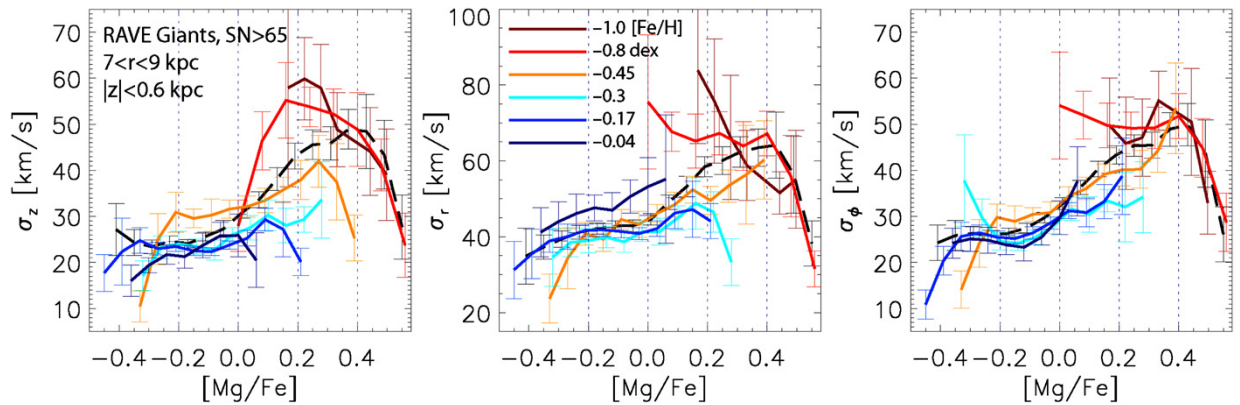


Figure 19: The results obtained by [1] are reproduced here.

4 Toy Model

We set up a toy model to investigate how measurement errors might alter the appearance of sharp increases in σ with $[\text{Mg}/\text{Fe}]$. The distribution of x values (representing ages of stars or $[\text{Mg}/\text{Fe}]$) is shown in Figure 20. y represents a velocity component of the star. In Figure 21, this should be thought of as the asymmetric drift. In Figure 22, the mean value of this velocity component is fixed at 0 so one can imagine it representing σ_R or σ_Z .

We determined y values for each ‘star’ by either setting it equal to the mean value of y corresponding to the x value (no dispersion) or by drawing it randomly from a normal distribution with zero mean and dispersion dependent on x according to a pre-determined relation. Next, we added a ‘measurement error’ to the x values but not to y . This involved simply adding a Gaussian random variable with constant dispersion of 1.5 to all the x values. The resulting mock dataset was then analysed using a Monte-Carlo procedure, similar to how we analysed actual data. We used 100 runs, each time adding a Gaussian random variable with dispersion 1.5 to all ‘measured’ values of x . The binning procedure applied to the mock data was the same as that used for real data.

The error in x we used is actually fairly small. If $[\text{Mg}/\text{Fe}]$ is distributed over a range of ~ 0.7 and the measurement error is ~ 0.1 (which is probably too small) then we should use $\Delta x = 2$. More conservative assumptions about errors in the RAVE data would correspond to even larger Δx . The number of stars in our toy model is an order of magnitude larger than in our sample. Thus, the obscuration of the striking underlying feature in our toy models due to measurement errors may be even larger in actual data, especially when one considers that the toy model assumes all velocity measurements are perfect. However, actual data may have a more equal distribution of stars amongst different $[\text{Mg}/\text{Fe}]$ values - the toy model is illustrative only.

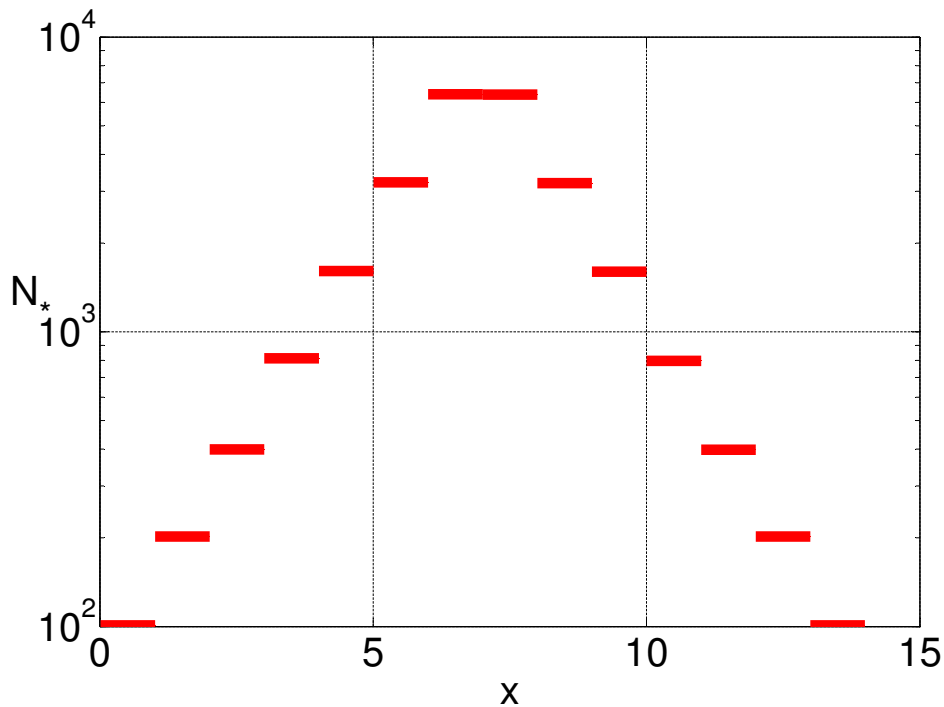


Figure 20: Distribution of actual x values in the toy model.

One clear outcome is that the gradient in the $\sigma_y - x$ or $\bar{y} - x$ relation will definitely appear smaller in the final analysis than in the underlying values. This is due to bins with values of x near the limits being swamped by stars with central values of x . The crucial feature of our model that makes this a significant effect is that there are many more stars in the central bins and measuring even a small fraction of them to have much lower or higher values of x would greatly affect results in the bins where these stars erroneously

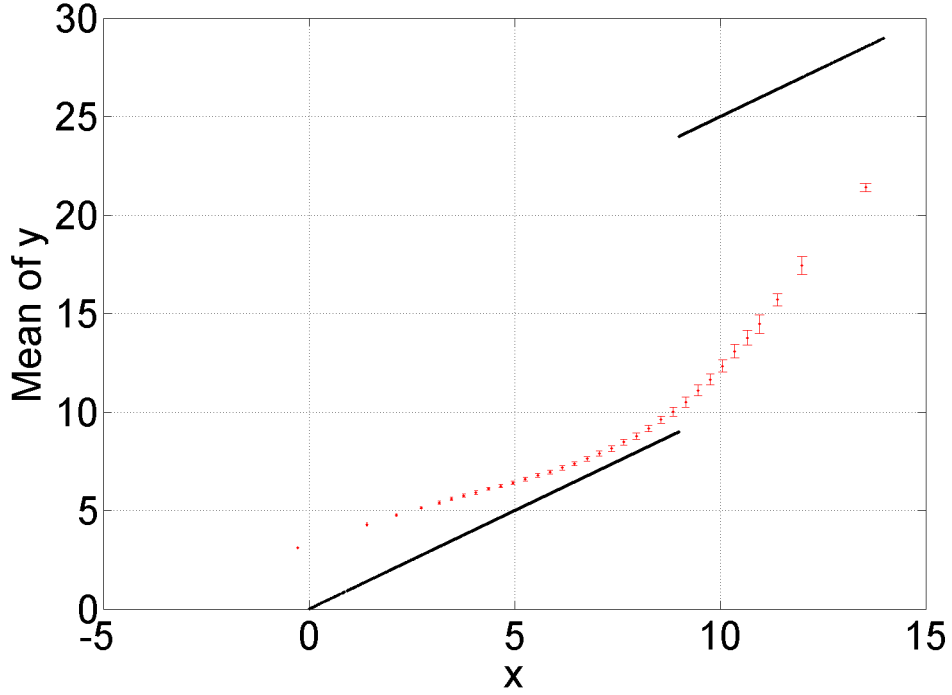


Figure 21: Mean y values resulting from a Monte-Carlo analysis of mock data. The underlying relation is shown as the solid line. $\Delta x = 1.5$.

end up. This leads to the values or dispersions obtained in any bin being driven towards those in the central bins, reducing any gradients that may be present.

The event was at $x = 9$ in our toy model, but even values as high as 11 lead to not much change in the appearance of the data. However, an event at even higher x will be difficult to confirm unless the data is substantially more accurate. This is due to the very small number of stars in bins with such high x . For galactic archaeology, this suggests that discerning events very early in the history of our galaxy may prove difficult if very few stars have survived from such periods. Then, even a fraction of younger stars being measured as old as those stars would seriously compromise the science.

Figures 21 and 22 show the effect of errors in the measurement of x on the feature in the underlying values. This feature is designed to correspond to stars older than 9 Gyr experiencing a jump in their velocity dispersion and asymmetric drift, with all stars experiencing secular heating at a uniform rate as well. As expected, this feature is smoothed out by measurement errors and no longer appears sharp. The interesting thing is the similar appearance to actual data (e.g. Figure 11, blue line). This could well be hiding sharp increases in velocity dispersion. Figure 23 suggests that it must show up if the error budgets in $[\text{Mg}/\text{Fe}]$ measurements are reduced to around one-thirtieth of their full range of values, corresponding to 0.03. It is likely the feature would be noticeable with slightly lower accuracy, especially if the distribution of $[\text{Mg}/\text{Fe}]$ values was more equal.

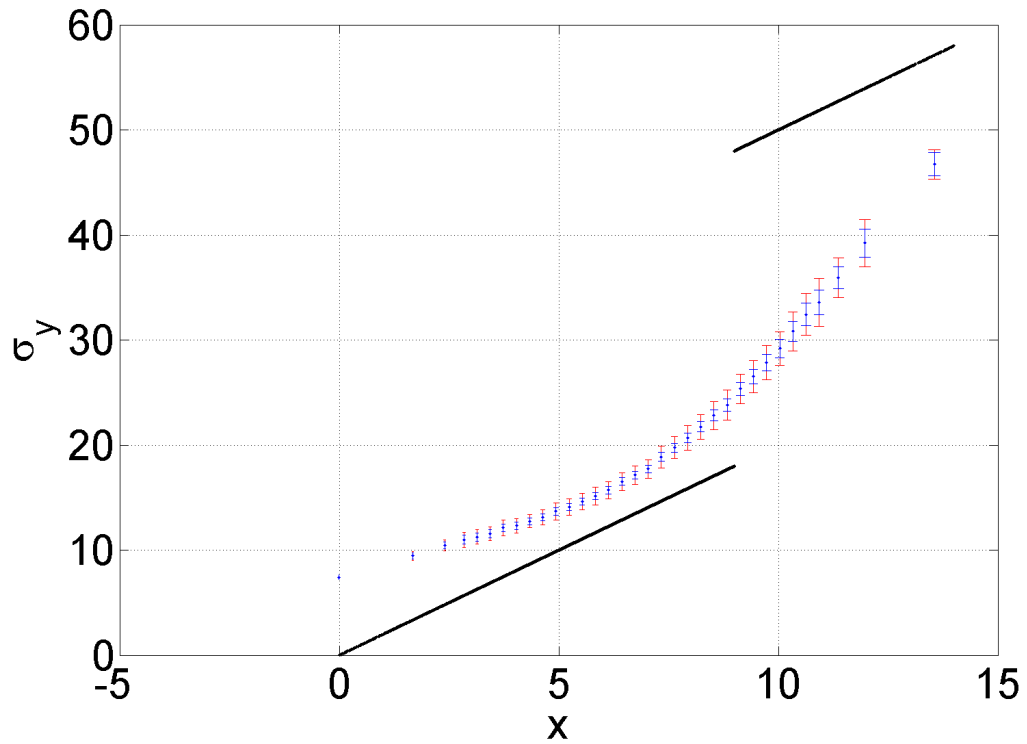


Figure 22: Dispersion in y values resulting from a Monte-Carlo analysis of mock data. The underlying relation is shown as the solid line. Inner and total error budgets have the same meaning as previously. $\Delta x = 1.5$.

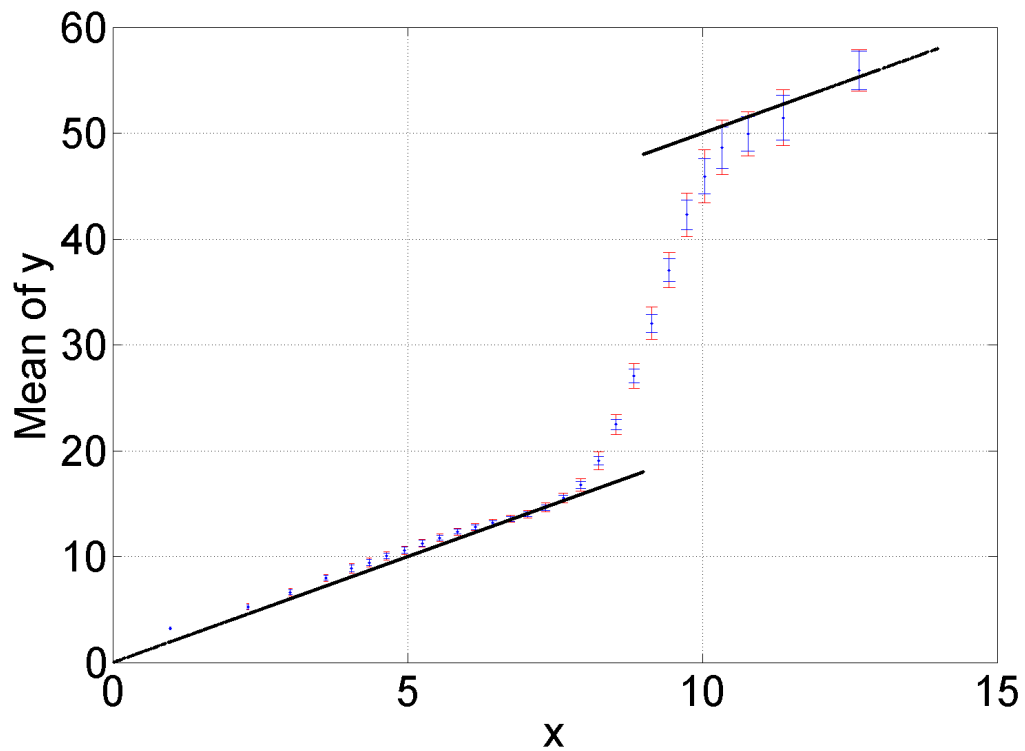


Figure 23: Δx has been reduced to 0.5, making the issue of cross-contamination much less problematic. The feature at $x = 9$ is now completely obvious.

5 Discussion

Our data do not show any sudden increase in velocity dispersion with $[\text{Mg}/\text{Fe}]$ similar to that found by [23], which used distances measured directly using trigonometric parallax. Partly because our distances are not, our data is less accurate but has much more stars. The toy model shows that such features could actually be present in the data and contributing to the accelerated increase of σ with $[\text{Mg}/\text{Fe}]$ at high values, especially when restricting attention to certain ranges of metallicity. If so, the heating event occurred at higher $[\text{Mg}/\text{Fe}]$ than the σ - $[\text{Mg}/\text{Fe}]$ relation appears to accelerate. This is because of measurement errors in $[\text{Mg}/\text{Fe}]$.

The results in Figure 11 appear to show an acceleration in the σ_Z - $[\text{Mg}/\text{Fe}]$ relation close to $[\text{Mg}/\text{Fe}] = 0$. This may be a sign of a sharp increase in σ , but if so this would have occurred at slightly higher values. Adding $\sqrt{2}$ times the measurement error in $[\text{Mg}/\text{Fe}]$ suggests it was ≈ 0.2 at that time. The most important constraint may come from the fact that the thick disk appears to be present at $[\text{Mg}/\text{Fe}] = 0.05$, when considering the lowest metallicity subsample. Adding the measurement error suggests that it was formed at $[\text{Mg}/\text{Fe}] \approx 0.25$. However, the data have been binned and only the mean $[\text{Mg}/\text{Fe}]$ value is plotted, so the data for this subsample extend to slightly lower $[\text{Mg}/\text{Fe}]$ and the estimate of 0.25 should be lowered accordingly. If the error budgets in elemental abundances were not well estimated, this will also affect the timing of the event, with larger errors making it longer ago.

Our results seem consistent with a sharp increase in velocity dispersion at $[\text{Mg}/\text{Fe}] \approx 0.2 - 0.3$, leading to the formation of the thick disk. The heating event seems to have been more efficient at larger radius. This is unusual for internal evolutionary processes as the surface density of the galaxy is lower at larger R , suggesting less efficient disk heating. Today, for example, the central region of our Galaxy is a bulge with quite high velocity dispersion.

Therefore, we believe the heating event was not caused by processes internal to the Milky Way, but was caused by tidal forces due to another galaxy which, long ago, was nearby. This affects outer regions of our Galaxy more, because the force towards the perturbing galaxy differs more from the force towards it at the centre of the Milky Way. Thus, outer regions of our Galaxy end up with larger velocities relative to its centre, leading eventually to larger velocity dispersions (on a dynamical timescale of a few hundred Myr).

The results in Figure 11 appear not to show much heating of the thick disk stars (lowest metallicity subpopulation) after the initial heating event. This suggests a single event (or multiple events very little separated in time). It appears this occurred < 12 Gyr ago (so $[\text{Mg}/\text{Fe}]$ starts dropping below 0.4, requiring Type Ia SNe to enrich the ISM). It occurred much above 5 Gyr ago, when the Sun formed (if the Sun has typical $[\text{Fe}]$ and $[\text{Mg}/\text{Fe}]$ values - Figure 7 suggests this is not quite true). Thus, we suggest the event took place 7-11 Gyr ago, consistent with our proposed explanation (see Appendix).

Interactions between galaxies are often associated with large increases in the star formation rate. Searching for evidence of this in the $[\text{Mg}/\text{Fe}] - [\text{Fe}/\text{H}]$ relation would be very valuable, although it may require much tighter error budgets on elemental abundances. Also important is whether, even in the outer regions, the heating caused by the event was uniform or whether substantial parts of the thin disk were largely unaffected. The Appendix explores a flyby of Andromeda and gives reasons to expect that the latter is true. However, a merger relies on gradual loss of orbital energy to dynamical friction and would likely affect most of the thin disk over repeated close passages to our Galaxy, even if only a part of it was affected on each close passage. This may lead to a different effect than a single fast flyby.

The radial density and mean metallicity profile of the thick disk may also hold important clues to its origin. Drawing out large amounts of gas to very large galactocentric distances and thereby forming perhaps most of the Milky Way's satellite galaxies would probably affect the thick disk in measurable ways, if this happened. In this case, determining the ages and properties of satellite galaxies may also give important insights. If the formation of the thick disk was caused by Andromeda, then observations of Andromeda should also reveal evidence of a major interaction at the same time as the thick disk of our Galaxy formed. Verifying this will require more accurate estimates of when this was, so more accurate elemental abundances of stars in the LSN will be critical in the future. Also important will be a better way to convert chemical abundances into ages, likely requiring improved understanding of the chemical enrichment history of our Galaxy.

6 A Natural Scenario for the Formation of the Thick Disk

6.1 Dynamics of the Milky Way and Andromeda galaxies

Investigating the history of our galaxy is interesting because it is plausible for it to have suffered an external shock due to a close encounter with another galaxy ([17]). Mergers, especially with small satellite galaxies, seem likely. Perhaps such an event is ongoing with the Sagittarius dwarf spheroidal galaxy. Certainly, such events are an essential ingredient within the standard Λ CDM paradigm. They may be discernible billions of years later due to unusual patterns in data on velocities and chemical abundances.

The dark matter particle has never been found and the Λ CDM model faces a number of severe observational challenges at galaxy scales (see [15]). The huge acceleration discrepancies in galaxies (between Newtonian gravity applied to observed mass and the centripetal acceleration $\frac{v^2}{r}$) may be a clear sign of invisible matter surrounding galaxies. But it may also plausibly be due to a breakdown of Newtonian gravity at accelerations many orders of magnitude below those where it is known to work. This theory is known as Modified Newtonian Dynamics (see [30]).

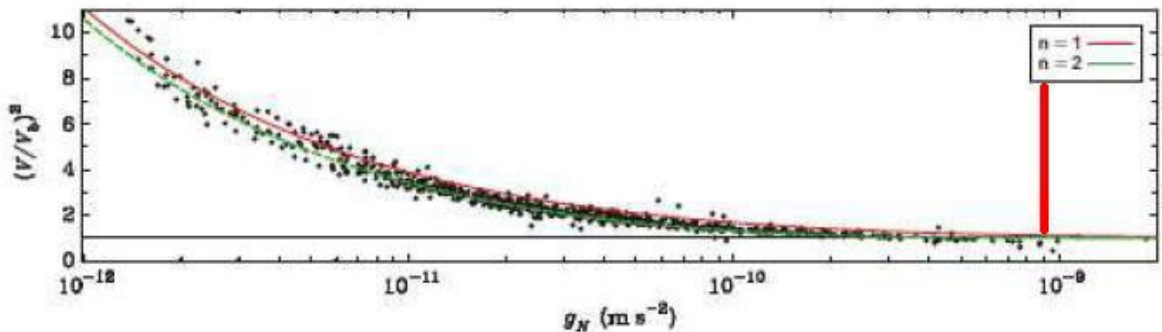


Figure 24: The ratio between true accelerations and that predicted by Newtonian gravity based on observed baryonic mass, as a function of the latter. Note that the energy density in a gravitational field ($\frac{g^2}{8\pi G}$) is smaller than ρ_{vac} (assumed to underlie the dark energy) if $g < 9.4 \times 10^{-10} \text{ m/s}^2$ (vertical line). Quantum gravity effects may become important at such low energy densities. MOND suggests the strong correlation present in this data be interpreted as an acceleration-dependent modification to Newtonian gravity. The graph is reproduced from [15].

Some of the strongest evidence for this comes from observations of our own galaxy and Andromeda. The highly anisotropic distributions of satellite galaxies appear unlikely in Λ CDM (see [8]). An origin in an ancient encounter with another galaxy is much more likely. However, such encounters lead to separation of baryonic and dark matter (see [29]). Consequently, the acceleration discrepancies in the satellite galaxies must be due to something else. As they are not all being tidally disrupted and some should really be in equilibrium and dynamically relaxed, the problem is most logically interpreted as due to a breakdown of Newtonian gravity. Indeed, a fit to Figure 24, if interpreted as an actual breakdown in Newtonian gravity (as done in MOND), would lead to substantially stronger gravity in the satellite galaxies of Andromeda. This appears to remove the need for any invisible mass (see [14]).

With such a substantial modification to gravity, the history of the local group may look very different (see [5]). Consequently, we integrated the orbit of Andromeda backwards in time to 1 Gyr after the Big Bang with both Newtonian gravity and MOND. As the time period is long and the distances large, an allowance must be made for cosmic expansion. However, this turns out to be relatively small except at very early times. Treating the MW and M31 as point masses, the governing equation is

$$\ddot{\vec{r}} = \vec{F} + \frac{\ddot{a}}{a} \vec{r} \quad (13)$$

a is the scale factor of the Universe and \vec{r} is the separation vector between the galaxies. \vec{F} is the vector sum of the accelerations due to each galaxy on the other. This is directed between them, so we deal only with the magnitude of F . In Newtonian gravity, this is given by

$$F = \frac{GM}{r^2} \quad (14)$$

$$M \equiv M_{MW} + M_{And} \quad (15)$$

The expression is more complicated in MOND, because the external gravitational field due to the rest of the Universe can affect the internal dynamics of a system. This feature of the theory is required for internal consistency, although it violates the Strong Equivalence Principle. Although the direction of the external field as well as its magnitude are relevant, we perform an interpolation between three limits in which F is analytic in MOND. These follow from consideration of the governing equation, the Modified Poisson Equation.

$$\nabla \cdot \left(\mu \left(\frac{|\vec{g}|}{a_0} \right) \vec{g} \right) = -4\pi G\rho \quad (16)$$

$$\mu(x) = 1, x \gg 1 \quad (17)$$

$$\mu(x) = x, x \ll 1 \quad (18)$$

$$(19)$$

The Newtonian limit is obtained when the galaxies are very close to each other, such that $F \gg a_0$. The deep-MOND limit arises when F greatly exceeds any external gravitational field upon the system ($F \gg g_{ext}$) but is much weaker than a_0 . In this limit, $F \propto \frac{1}{r}$. The external field-dominated limit arises when $F \ll g_{ext}$. In this case, the external field fixes the value of the μ function, leading to a rescaled version of the usual Poisson Equation and an inverse square force law. However, if $g_{ext} \ll a_0$, the force can be much larger than in Newtonian gravity. This is called the quasi-Newtonian regime, and will be very relevant here.

$$F = \frac{GM}{r^2} \left[1 + \frac{1}{\frac{\sqrt{GM}}{rQ\sqrt{a_0}} + \frac{g_{ext}}{a_0}} \right] \quad (20)$$

$$q_i \equiv \frac{m_i}{M} \text{ where } i \text{ labels the galaxies} \quad (21)$$

$$Q \equiv \frac{2 \left(1 - q_1^{\frac{3}{2}} - q_2^{\frac{3}{2}} \right)}{3q_1q_2} \quad (22)$$

$$(23)$$

Over a substantial part of the orbit, F approximately follows the deep-MOND limit.

$$F = \frac{Q\sqrt{GMa_0}}{r} \quad (24)$$

When the galaxies are near their greatest separation, the external field-dominated (quasi-Newtonian) limit becomes a good approximation.

$$F = \frac{GM}{r^2} \times \frac{a_0}{g_{ext}} \quad (25)$$

Consequently, despite the $\frac{1}{r}$ behaviour of the force in MOND being the original motivation for the theory, it is possible for particles to escape from a finite mass as there are always other masses in the Universe. In

fact, due to large scale structure, g_{ext} probably always exceeds $0.01a_0$. Thus, it is possible for the Milky Way and Andromeda to be unbound and for particles to escape from these galaxies. Indeed, a calculation of the escape speed from the Milky Way made in this way ([32]) agreed closely with the value obtained from a recent analysis of high velocity stars in our galaxy using RAVE DR4 ([31]).

Using the governing equations of MOND, the external field on the Milky Way-Andromeda system can be constrained using the escape speed from our Galaxy. However, this is difficult because a large part of the external field on it is due to Andromeda, making the contribution from more distant objects hard to constrain. Instead, the value of g_{ext} and its time history may be estimated based on the fact that it needs to be consistent with the presently observed peculiar velocity of the local group with respect to the surface of last scattering ([4]). Assuming for simplicity that g_{ext} does not change direction, the governing equation for peculiar velocities (explained later in this section) is

$$\dot{v} = -Hv + g_{ext} \quad (26)$$

For simplicity, we assume that $g_{ext} \propto (1+z)^{0.8}$, treating the external field as due to a distant point mass which was slightly less in the past. Of course, g_{ext} will end up higher in the past, but we need to make it vanish at early enough times (when there was no structure). This is effected by integrating the above equation back in time and finding when $v_{pec} = 0$. At earlier times, the external field is switched off. For the g_{ext} parameterisation to be reliable, we need this to happen several Gyr after the Big Bang, to allow for low values of g_{ext} at early times, when not much structure had yet formed. Very high values of g_{ext} would lead to v_{pec} dropping to 0 too recently for the model to be realistic (e.g. implying negligible structure within the first 8 Gyr of the Universe's history). We suggest using $g_{ext} = 0.0155 a_0$ at the present epoch, forcing $g_{ext} = 0$ before 1.9 Gyr after the Big Bang. Although the resulting model is not totally realistic, it probably overestimates g_{ext} and so underestimates the force between the galaxies) at early times.

Parameter	Value
Milky Way - Andromeda distance today	770 kpc
Radial velocity of Andromeda	109.3 km/s (error about 4)
Tangential velocity of Andromeda	17 km/s (error about 17)
M_{MW} , MOND	$0.7 \times 10^{11} M_{\odot}$
M_{And} , MOND	$1.6 \times 10^{11} M_{\odot}$
M_{MW} , Newton	$2 \times 10^{12} M_{\odot}$
M_{And} , Newton	$2.5 \times 10^{12} M_{\odot}$
a_0	$1.2 \times 10^{-10} \text{ m/s}^2$
g_{ext}	$0.0155 a_0 \times (1+z)^{0.8}$
H_0	$67.3 \text{ km s}^{-1}/\text{Mpc}$
Ω_m	0.315

Table 4: Parameters used in simulations of the past orbit of Andromeda. A standard expansion rate history is assumed. The velocity vector of Andromeda is obtained from [37].

The simulations we performed suggest that a past encounter between the MW and M31 is essentially unavoidable, with a closest approach distance below 55 kpc and probably closer to 20 kpc. This uncertainty is driven primarily by the proper motion of Andromeda. The time of the encounter would likely have been 3-5 Gyr after the Big Bang. In our model, raising the value of g_{ext} at the present epoch forces one to accept it was 0 until later times. This leads to a substantially larger force at early times (as external fields weaken the self-gravity of a system). This compensates for the weaker force at more recent times. Physically, a larger g_{ext} today must mean it was smaller in the past, to maintain the constraint on v_{pec} . Thus, it is almost impossible to find realistic choices of parameters in which a past encounter between the MW and M31 is avoided, if using Modified Newtonian Dynamics.

Such an encounter is impossible with Newtonian gravity because this automatically implies the existence of extended halos of dark matter. The resulting dynamical friction during an encounter would lead to a merger. However, we reran the simulations with the galaxy masses set at the high end (and a Newtonian force law). Considering that the masses were likely lower in the past (but not in our model) and also overestimated (e.g. [31]), it is very difficult to get an encounter between the galaxies in this theory.

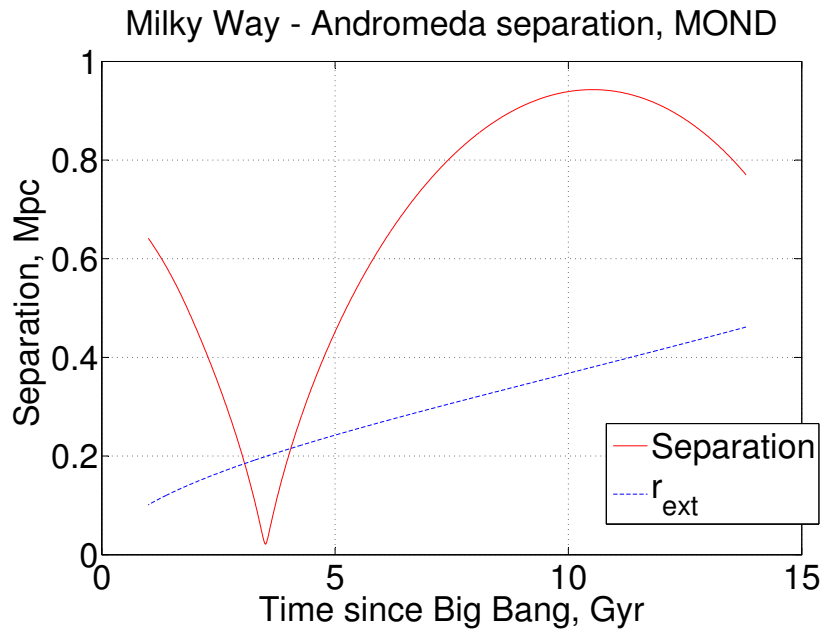


Figure 25: The solid line shows the distance between the Milky way and Andromeda galaxies, integrated backwards in time using MOND. The dashed line shows the separation beyond which the external field effect of large scale structure leads to a substantial weakening of the force between the galaxies. This force is still much larger than in Newtonian gravity if $g_{ext} \ll a_0$, as is the case here. This simulation gives a closest approach distance of just 21 kpc.

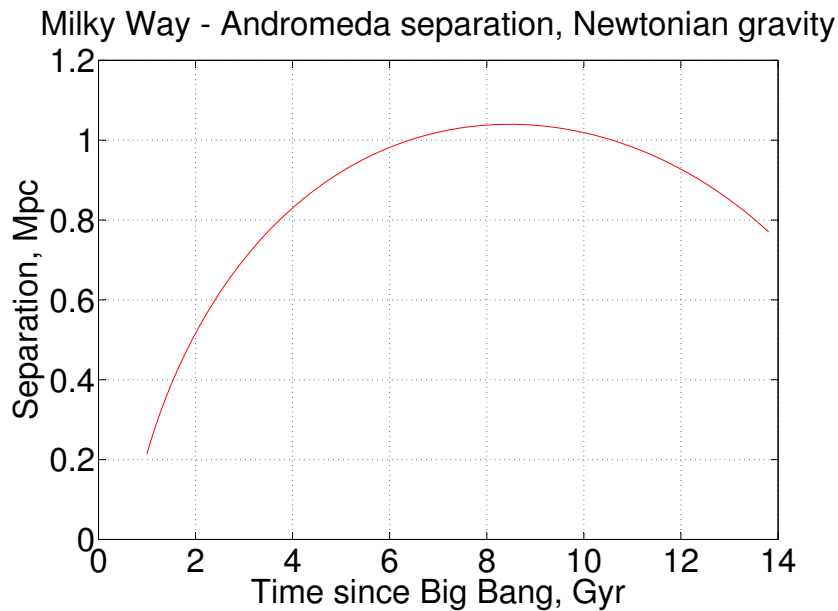


Figure 26: The separation between the Milky Way and Andromeda galaxies in Newtonian gravity, with masses at the high end of what is likely and staying the same into the past. It is unclear if the galaxies really existed in the first Gyr of the Universe's history, so we do not consider the possibility of an encounter then.

6.1.1 Dynamics in an Expanding Universe

A freely falling observer not co-moving with the Hubble flow experiences a Hubble drag

$$\dot{v}_{pec} = -Hv_{pec} \quad (27)$$

This can be proved by taking the position of the observer at some time to be the centre of the expansion. In this co-ordinate system, the instantaneous velocity of the particle is by definition v_{pec} . At a slightly later time, the velocity of co-moving particles at the new position of the particle is $Hv_{pec}dt$, leading to the Hubble drag. If the observer is acted upon by a force, this is simply added to the right-hand side of the equation.

Now, we determine the velocity as seen by a co-moving observer far from the trajectory of the particle. We treat the problem as effectively one dimensional.

$$v = Hd + v_{pec} \text{ so that} \quad (28)$$

$$\dot{v} = H\dot{d} + \dot{H}d + \dot{v}_{pec} \quad (29)$$

$$= H\dot{d} + \dot{H}d - Hv_{pec} \quad (30)$$

$$= H(Hd + v_{pec}) + \dot{H}d - Hv_{pec} \quad (31)$$

$$= (\dot{H} + H^2)d \quad (32)$$

$$= \left(\frac{\ddot{a}}{a} - \frac{\dot{a}^2}{a^2} + \frac{\dot{a}^2}{a^2} \right) d \quad (33)$$

$$= \frac{\ddot{a}}{a}d \quad (34)$$

$$(35)$$

Thus, the relative cosmological acceleration between two objects is directed along a line joining them and tries to make them accelerate apart if $\ddot{a} > 0$, as is the case presently.

6.2 The Geometry of a Flyby of Andromeda

Figure 27 shows measurements of the crucial 3D vectors needed to determine the dynamics of the Milky Way and Andromeda galaxies. The present orbital pole of the orbit of M31 is poorly constrained ([37]), though the known position of M31 forces this to lie along a Great Circle. However, we can guess where the orbital pole lies, as follows. An encounter provides a natural explanation for the anisotropic distributions of satellite galaxies around the MW and M31 (see [9] and [10]). This appears difficult to reconcile with the Λ CDM paradigm (see [8]), which requires these galaxies to not be generated in a tidal interaction due to their high inferred dark matter content ([29]). This suggests the model is inconsistent with observations, so we consider MOND instead.

In this theory, an ancient interaction between the Milky Way and Andromeda is inevitable (see Appendix 6.1 and [5]), so the tidal tails generated during it may have formed the anisotropically distributed satellite galaxies around the MW (the VPOS) and M31 (the VTDS). If so, then the angular momentum vector of the satellite galaxies is a linear combination of that due to the host galaxies' orbit and their internal spin (as this determines the initial angular momentum of the gas). This suggests guessing the present orbital pole of M31 by drawing a line from the disk spin vectors of the galaxies through the orbital pole preferred by their satellite distributions and carrying on a little further (because e.g. the VPOS orbital pole preferred by MW satellites should lie somewhere between the MW disk spin and the M31 orbital pole). 'Triangulating' in this way (suggested by Pavel Kroupa, [38]), one ends up at somewhere around $l = 0$, $b = 50^\circ$ as the likely pole of the M31 orbit. This is well within the uncertainty on the measurement of this vector (see Figure 27).

The direction to M31 at the time of the flyby can now be estimated given the azimuthal angle traversed by M31 in its orbit around the MW since the time of the flyby. The change in velocity during the encounter can be estimated analytically by adding $\frac{\pi v_f^2}{v}$ for both galaxies and setting $v = 550$ km/s, the escape speed from the MW ([31]). This suggests $\Delta v = 475$ km/s. This is added orthogonally to the original relative velocity. Also, the magnitude of the relative velocity is unchanged (energy conservation). Consequently, we expect a deflection angle of $60^\circ (= \sin^{-1}(\frac{475}{550}))$. Adding half of this to the result for an undeviated trajectory (90°), we get $\sim 120^\circ$.

Much more accuracy can be obtained by running a simulation as described in Section 6.1 (and using $\dot{\phi} = \frac{h}{r^2}$). This shows that the angular distance traversed by M31 since the flyby is 126° , with the relatively large uncertainty on the present tangential speed of M31 only affecting this by a few degrees. This is because the speed at the time of closest approach is almost unchanged at around 610 km/s and the deep-MOND result for the impulse-approximation deflection angle is independent of the distance of closest approach (which, however, *is* very sensitive to the orbital angular momentum of M31). The principal reason for the increase in angle compared to the analytic approximation is that the encounter is not very far into the deep-MOND regime, and (if g_{ext} is unimportant) the gravitational force is always stronger than the deep-MOND result. The trajectory is also not that close to a straight line, as assumed.

Rotating the direction to M31 by -126° to turn the clock back to the time of the encounter, we see that the direction to M31 at this time was approximately $l = 0$, $b = 42^\circ$. The velocity of Andromeda can be found based on the fact that, at the point of closest approach, the direction from the MW to M31, its velocity relative to the MW and its orbital angular momentum were all orthogonal to each other. Thus, $\vec{v} \propto -\vec{r} \times \vec{h}$. This gives a direction approximately along $l = 90^\circ$, $b = 0$.

At this time, the effect of Andromeda on the Milky Way would have been substantial. Yet, it is only the *difference* in the impulse exerted on different parts of the Milky Way that is of relevance here - the motion of the centre of mass of the MW will not affect its internal properties. Thus, we need to consider tidal forces.

We assume the encounter took place at a distance of 22 kpc (between the centres of the galaxies) and treat Andromeda as a point mass. Next, we consider test particles located at the centre of the MW and at two points within its disk plane 8 kpc from its centre (we take the extent of the MW disk to be 8 kpc). We ignore the gravity of the MW on these test particles (it will be clear later that this is a reasonable assumption - at least in the outer parts of our Galaxy - partly because Andromeda is more massive than the Milky Way). One of the test particles is the closest part of the MW to M31, while the other is at right angles to this direction (within the MW disk plane). This should give a reasonable idea of the tidal velocity (i.e. relative to the particle at the centre of the MW) that is imparted by the flyby. We treat Andromeda as going in a straight line at constant speed during the encounter and use the impulse approximation valid for a weak encounter. The results obtained in this way will not be exact.

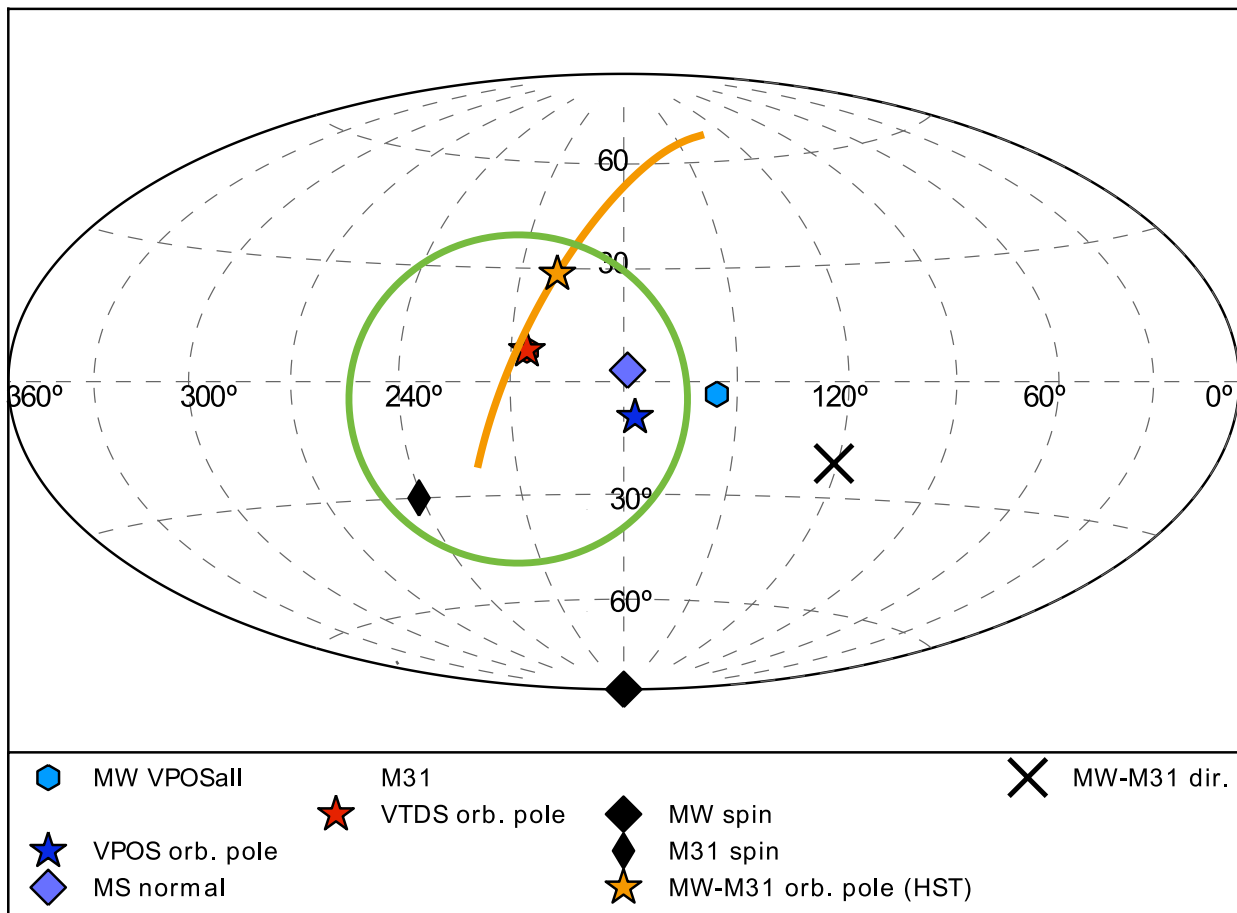


Figure 27: Important directions are illustrated here in galactic co-ordinates. The red star is the orbital pole of the VTDS (an anisotropic system of satellite galaxies orbiting M31). The blue star is the same for the VPOS (a similar system around the MW). The present orbital pole of the orbit of M31 around the MW is along the orange line (an error bar), with the orange star at its centre the most likely location ([37]). The black diamonds are the disk spin directions of the MW (by convention at a galactic latitude of -90°) and M31. The present direction to M31 is the black cross. Figure reproduced from [36].

The magnitude of the impulse exerted by M31 on all these particles is roughly the same (slight differences arising because the deep-MOND assumption is only weakly valid). The important effect is that the impulses are in different *directions*. For each particle, one must determine the point along the (straight line) trajectory of M31 at which it is closest. The direction from the particle to this point is the direction of the impulse (we treat the particles as static and M31 as moving).

Figure 28 shows two particles in the MW disk, one at its centre and the other as close as possible to M31 at the time of its closest approach (to both O and A). The particle at A gains a net velocity (i.e. relative to the particle at O) because of the difference in directions to M31. However, a particle in the MW disk which is located orthogonally to A experiences very little net impulse.

Figure 29 illustrates particles along the line in the MW disk most closely aligned with the velocity of M31. The impulse on these particles is in the same direction (BB'). Now, the magnitude is distance-independent in the deep-MOND regime and the distances BB' and CC' are nearly equal (as our simulations suggest very little angle between BC and B'C'). For both these reasons, the impulse on all particles along BC should be very similar in magnitude. Thus, they suffer little tidal heating. The importance of some parts of the Milky Way being tidally heated much less than others will be discussed below.

Assuming the magnitude of the impulse exerted by M31 is ~ 300 km/s (to include the effect of not being

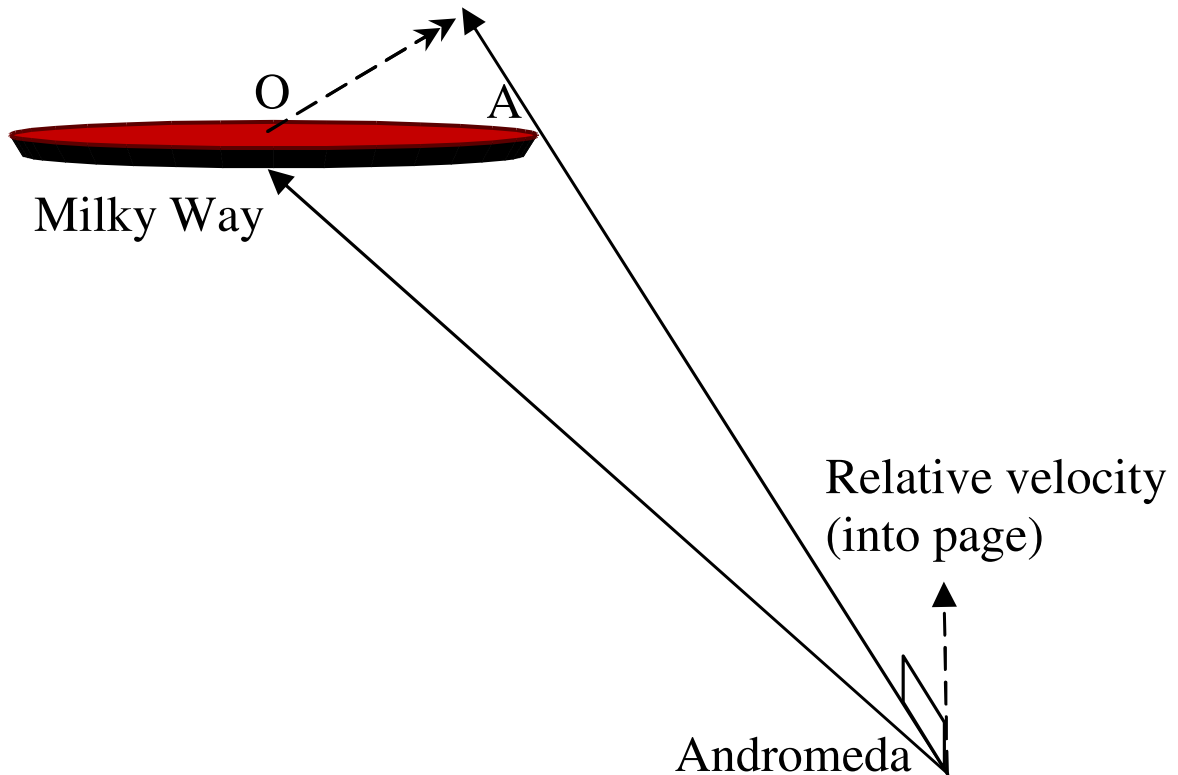


Figure 28: The velocity of M31 is orthogonal to the plane of the paper, so the point at which it approaches particles O and A closest is the same. Pretending the impulse is directed from this point *towards* O and A and that the impulse has equal magnitude in both cases, we are forced to extend the vector to A further to get the same length as the vector to O. This means the particle at A receives an extra (vector) impulse - above what the particle at O experiences - in the direction of the double arrow. In reality, this would be in the opposite direction. Crucially, the flyby is capable of inducing a net velocity at A orthogonal to the MW disk plane.

fully in the deep-MOND regime), basic geometry shows that the net velocity of the particle at A will be ~ 100 km/s and inclined by $\sim 40^\circ$ to the MW disk. This leads to a vertical velocity of ~ 65 km/s. One is also left with a radial velocity (i.e. directly towards O) of ~ 75 km/s, but no tangential velocity (beyond that originally present). In reality, these values will be slightly larger as the impulse exerted at A is slightly larger than at O, as the system is only marginally in the deep-MOND regime.

After the flyby, the particle (which is orbiting the Milky Way) will reach smaller galactocentric radii and be forced to increase its tangential speed v_ϕ around the MW to conserve angular momentum. This leads to a tangential velocity dispersion after a few hundred Myr. The vertical velocity would lead to the excitation of epicyclic motions in the vertical direction. Assuming the vertical velocity then varies sinusoidally, the resulting velocity dispersion is $\frac{1}{\sqrt{2}}$ times the maximum vertical velocity, yielding $\sigma_Z \approx 45$ km/s.

The timescale for the flyby is ~ 70 Myr, much shorter than the orbital period of stars in the MW at the solar radius (~ 220 Myr). Thus, the flyby is relatively fast on orbital timescales (justifying our earlier assumption). Material can remain within a narrow range of angles around the galaxy for the duration of the flyby (especially in the outer parts of the MW). Consequently, some material will inevitably be in the direction orthogonal to OA and not experience much tidal heating. This may have important observational consequences.

In this model - which appears to yield realistic results - the thick disk formed well after a thin disk had already been established. Yet, there should still be stars in the thin disk which predate the flyby. A merger, while qualitatively similar, requires repeated passages of another galaxy while its orbital energy is dissipated via dynamical friction on each passage. This leaves little chance for any part of the thin disk to not get

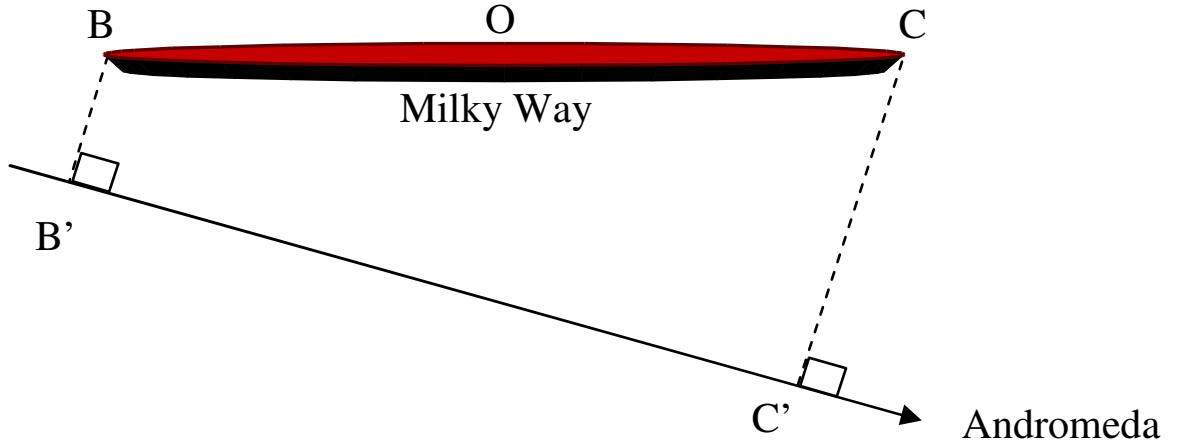


Figure 29: The plane of the paper contains both the velocity of M31 and the direction in the MW disk plane most closely aligned with that direction. Closest approach to B occurs when Andromeda is at B' (analogous for C and C'). Note that BB' and CC' are parallel, so the impulse on B and on C is in the same direction. Because the magnitude of the impulse is independent of the distance of closest approach in the deep-MOND regime (see later), the impulse on all particles along the line BC will be similar. There will be little tidal heating. This is especially true if BC and B'C' are nearly parallel, as simulations suggest.

Parameter	Value
Orbital pole of M31 orbit around the MW	$l = 0, b = 50^\circ$
Angular motion of M31 around MW since the flyby	126°
Present direction to Andromeda	$l = 120^\circ, b = -20^\circ$
Distance of closest approach	22 kpc
Size of Milky Way disk	8 kpc

Table 5: Parameters used to determine the encounter geometry.

dynamically heated. Thus, the thin disk would be unlikely to have a substantial number of stars predating the formation of the thick disk in such a scenario.

In our model, the thick disk would contain both stars and gas. Some of the gas would be drawn into long tidal tails on a polar orbit around the MW, eventually forming tidal dwarf galaxies which we observe today as the VPOS (see [33]). Because of this high inclination, the gas could not efficiently settle down into a thick disk co-rotating with the thin disk. Thus, there would be ample time for stars to be formed from the gas. In fact, if the MW was very gas-rich at these early times, most of the stars in the thick disk may have formed from gas that was raised onto inclined orbits during the flyby rather than have already been formed in the pre-existing thin disk.

With dynamical times much longer than the ~ 70 Myr duration of the flyby, especially in the outer parts of the MW, the formation of tidal tails would be likely. This requires a sustained force on dynamically cold material, and a heavy galaxy flying past a gas-rich one which is slow-rotating (on the relevant timescale) provides nearly ideal conditions for this to occur. This would lead to gas being taken out of the newly formed thick disk, some of this ultimately forming the satellite galaxies in the VPOS or even around M31. The loss of gas from the outer parts of the thick disk may lead to a reduction in its scale length, especially as the inner few kpc have a dynamical time below the flyby duration and are less strongly affected by tides. Thus, the loss of gas from such regions less likely.

If gas indeed went onto a nearly polar orbit around the Milky Way (by gaining some of the orbital angular momentum of M31 due to tidal torques) but some of it did not get very far from the MW, then it would be difficult for this to settle down again with an angular momentum aligned with the thin disk. This gas would repeatedly lose energy on disk crossings, until eventually perhaps it would end up at very small galactocentric radii. Here, it may contribute to the bulge or further raise the density in the inner regions

of the thick disk. Combined with the fact that material at A will be pushed towards smaller galactocentric radii (where it may dissipate its excess tangential speed and settle on a circular orbit), there are several good reasons why the thick disk may have a shorter scale length than the thin disk out of which it formed.

The excitation of large radial velocities during the flyby may lead to efficient mixing of material in the MW and reducing any gradients in e.g. metallicity with galactocentric radius. However, in the ~ 9 Gyr after the flyby, when perhaps most of the stars in the MW actually formed, the higher density of stars closer to the centre should still lead to more efficient enrichment of the interstellar medium there. Thus, stars born there should have a higher metallicity than stars born further out, at the same time. There should be ample time to re-establish a radius-metallicity relation after the flyby. In fact, the galaxy must have been very gas-rich if the VPOS and VTDS were really generated during this event. The fact the MW is not gas-dominated today suggests that a substantial amount of star formation took place after the flyby, consistent with the present rate of star formation and the billions of years elapsed since the flyby.

The thick disk, however, does not appear to have undergone a substantial amount of star formation for billions of years. The lower gas density within it may mean that only with the shocks generated during the flyby was it able to efficiently form stars. If this is so or if star formation ceased not long after the flyby for other reasons (e.g. exhausting the gas), then there is much less chance of re-establishing a radius-metallicity relation. Consequently, the radial gradients of the chemistry of stars may be very different in the thin and thick disks, in the sense of gradients being weaker in the thick disk. Observations which can determine whether this is the case would thus be very valuable.

6.2.1 The Impulse Approximation in the Deep-MOND Limit

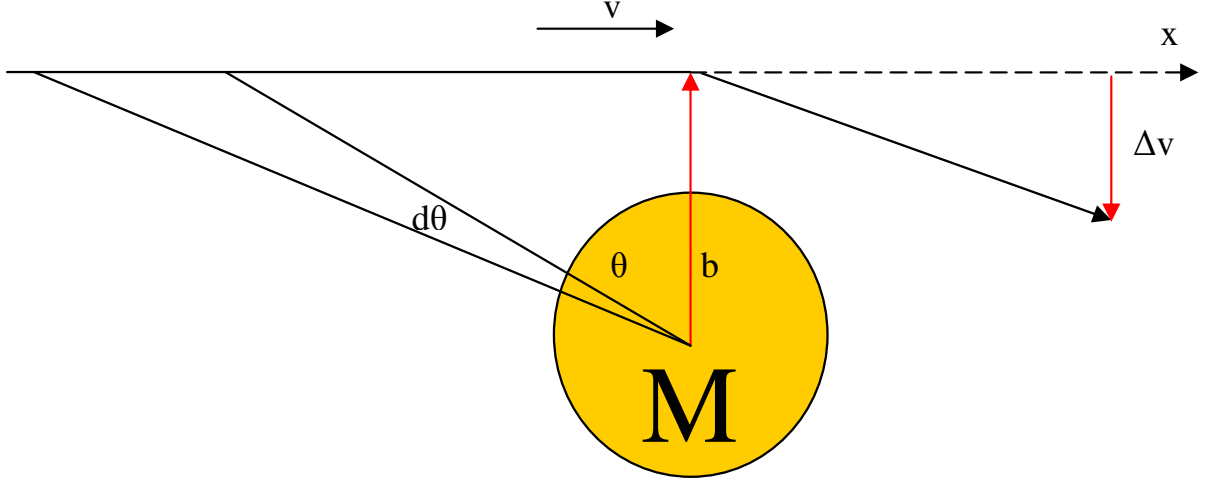


Figure 30: A test mass moves at speed v and impact parameter b subject to the gravitational force from a point mass M . The position of the particle is given approximately by $x = vt$, with $t = 0$ at the time of closest approach.

Consider a test particle moving at speed v in the gravitational field of a larger object of mass M . The trajectory has impact parameter b . Suppose the particle is deviated only slightly from its original path, so that the trajectory is given by $x = vt$ in Figure 30. Δv is determined by

$$\Delta v = \int_{-\infty}^{+\infty} F \cos(\theta) dt \quad (36)$$

These integrals usually require changing variable to θ , using $v dt = -b \sec^2 \theta d\theta$, with limits $\theta = \pm \frac{\pi}{2}$. The resulting change in velocity of the particle is directed from the point of closest approach towards the (fixed) mass. In Newtonian gravity, the magnitude of the impulse is given by

$$\Delta v = \frac{2GM}{bv} \quad (37)$$

In the deep-MOND limit (where $F = \frac{\sqrt{GMa_0}}{r}$), the analogous expression is

$$\Delta v = \frac{\pi \sqrt{GMa_0}}{v} \quad (38)$$

$$= \frac{\pi v_f^2}{v} \quad (39)$$

For ease of comparison with observations, we used the relation $v_f = \sqrt[4]{GMa_0}$, as the asymptotic circular velocity around the mass (v_f) can often be determined. Note that the impulse is independent of the distance of closest approach (because the gravitational force $\propto \frac{1}{r}$ and the time spent near the mass $\propto r$). The deflection angle of the trajectory of the test particle is $\pi \left(\frac{v_f}{v}\right)^2$, using a small angle approximation. For larger deflections, one should use the arcsine of this, because the speed of the particle is the same before and after the encounter (energy conservation) and our calculation approximately gives the velocity orthogonal to the original direction of motion.

The approach outlined here will not work well for deflections through a right angle or larger as the forces should be evaluated along the actual trajectory rather than the undeviated one & the distinction becomes important.

7 Conclusions

Based on a Monte-Carlo analysis of a sample of ~ 13000 stars from RAVE DR4 and comparison with a toy model, we find evidence for a relatively rapid heating event which likely formed the thick disk. This is consistent with results obtained from ~ 200 stars with parallax measured by Hipparcos ([23]). A correlation is apparent whereby stars at smaller galactocentric radii (R) were heated less. Some stars born there then migrated into the solar neighbourhood. As the density is higher at lower R , internal disk heating mechanisms will generally be more efficient there, not less. Therefore, we believe the heating was caused externally, due to tides from another galaxy which was nearby at one time. Tidal forces would affect the outer parts of our Galaxy more.

Accounting for measurement errors, our data suggest the event occurred at $[\text{Mg}/\text{Fe}] \approx 0.2 - 0.3$. We do not rule out multiple events spaced closely in time (i.e. compared to the age of our Galaxy). We cautiously suggest the event occurred 7-11 Gyr ago and speculate that it was a close flyby of Andromeda. This scenario is likely on other grounds and is consistent with this age range. A key question in the future will be whether the event heated the outer regions of our Galaxy uniformly or if substantial portions of the thin disk were left largely unaffected, as seems likely in our scenario. Answering this question should better elucidate the nature of the event.

Apart from quality of data, the major limitation of this work is the indirect nature of both age and radius of birth estimates. Directly observing stars at smaller R will thus be very helpful, as will more accurate elemental abundances and methods to convert these into ages. Ongoing surveys are currently working towards these goals.

References

- [1] Minchev, I., Chiappini, C., Martig, M. et. al. 2014, ApJL, 781, L20
- [2] Gilmore, G. & Reid, N. 1983, MNRAS, 202, 1025
- [3] Matteucci, F. 2012, Chemical Evolution of Galaxies
- [4] Kogut, A., Lineweaver, C., Smoot, G. F. et. al. 1993, ApJ, 419, 1
- [5] Zhao, H., Famaey, B., Lughausen, F. et. al. 2013, A & A, 557, L3
- [6] M. E. K. Williams et. al. MNRAS 436, 101121 (2013)
- [7] Binney, J., Burnett, B., Kordopatis, G. et al. 2014, MNRAS, 437, 351
- [8] Ibata, R. A., Ibata, N. G., Lewis, G. F. et. al. 2014, ApJL, 784, L6
- [9] Ibata, R. A. et. al. 2013, Nature, 493, 62
- [10] Pawlowski, M. S. & Kroupa, P. 2013, MNRAS 435, 2116
- [11] Kordopatis, G., Gilmore, G., Steinmetz, M. et. al. 2013, AJ, 146, 134
- [12] Asplund, M., Grevesse, N. & Sauval, A. J. 2005, ASP Conference Series, 336, 25
- [13] Matijevic, G., Zwitter, T., Bienayme, O. et.al. 2012, ApJS, 200, 14
- [14] McGaugh, S. & Milgrom, M. 2013, ApJ, 766, 22
- [15] Famaey, B. & McGaugh, S. 2012, Living Rev. Relativity, 15, 10
- [16] Eggen, O. J., Lynden-Bell, D. & Sandage, A. R. 1962, ApJ, 136, 748
- [17] Searle, L. & Zinn, R. 1978, ApJ, 225, 375
- [18] Schonrich, R., Binney, J. & Dehnen, W. 2010, MNRAS, 403, 1829
- [19] Schonrich, R. 2012, MNRAS, 427, 274
- [20] Schonrich, R., Binney, J. & Asplund, M. 2012, MNRAS, 420, 1281
- [21] Perryman, M. A. C., de Boer, K. S., Gilmore, G. et al. 2001, A & A, 369, 339
- [22] Wilson, M. L. et. al. 2011, MNRAS, 413, 2245
- [23] Quillen, A. C. & Garnett, D. R. 2001, ASP Conference Series, 230, 87
- [24] Sellwood, J. A. & Evans, N. W. 2001, ApJ, 546, 176
- [25] Carlberg, R. G. & Sellwood, J. A. 1985, ApJ, 292, 79
- [26] Minchev, I., Chiappini, C. & Martig, M. 2013, A & A, 558, A9
- [27] Ibata, R., Gilmore, G., & Irwin, M. J. 1994, Nature, 370, 194
- [28] Skrutskie, M.F. et. al. 2006, AJ, 131, 1163
- [29] Barnes, J. E. & Hernquist, L. 1992, ARA&A, 30, 705
- [30] Milgrom, M. 1983, ApJ, 270, 365
- [31] Piffl, T. et. al. 2014, A & A, 562, A91
- [32] Famaey, B., Bruneton, J. P. & Zhao, H. S. 2007, MNRAS, 377, L79

- [33] Pawlowski, M. S., Pflamm-Altenburg, J. & Kroupa, P. 2012, MNRAS, 423, 1109
- [34] Rubin, Vera C., Ford, W. Kent, Jr. 1970, ApJ, 159, 379
- [35] Wyrzykowski, L. et. al. 2011, MNRAS, 413, 493
- [36] Pawlowski, M. S., Kroupa, P. & Jerjen, H. 2013, MNRAS, 435, 1928
- [37] Sohn, S. T., Anderson, J. & Van der Marel, R. P. 2012, AJ, 753, 7
- [38] Kroupa, P. Private communication.
- [39] Feast, M. & Whitelock, P. 1997, MNRAS, 291, 683